Get Full Access and More at ExpertConsult.com

CT AND MRI OF THE WHOLE BODY

John R. Haaga | Daniel T. Boll Sixth Edition

40th ANNIVERSARY EDITION

VOLUME I

VOLUME II

ELSEVIER

2-Volume Set

CT AND MRI OF THE WHOLE BODY

VOLUME I

CT AND MRI OF THE WHOLE BODY

Sixth Edition

John R. Haaga, MD, FACR, FSIR, FSCBT, FSRS
Gold Medalist AARS and SCBTMRI
Professor of Radiology
Case Western Reserve University School of Medicine
Emeritus Chairman and Professor of Radiology
University Hospitals/Case Medical Center
Case Western Reserve University School of Medicine
Cleveland, Ohio

Daniel T. Boll, MD, FSCBT
Professor of Radiology
Section Chief Abdominal and Oncologic Imaging
University Hospital of Basel
Basel, Switzerland

ELSEVIER

ELSEVIER

1600 John F. Kennedy Blvd.
Ste 1800
Philadelphia, PA 19103-2899

CT AND MRI OF THE WHOLE BODY, SIXTH EDITION

ISBN: 978-0-323-11328-1
Volume 1 Part Number: 9996117383
Volume 2 Part Number: 9996117324

Library of Congress Cataloging-in-Publication Data

Names: Haaga, John R. (John Robert), 1945- , editor. | Boll, Daniel T., editor.
Title: CT and MRI of the whole body / edited by John R. Haaga, and Daniel T. Boll.
Description: Sixth edition. | Philadelphia, PA : Elsevier, [2017] | Includes bibliographical references and index.
Identifiers: LCCN 2016001268 | ISBN 9780323113281 (hardcover : international edition : alk. paper) | ISBN 9780801670572
Subjects: | MESH: Tomography, X-Ray Computed | Magnetic Resonance Imaging | Whole Body Imaging
Classification: LCC RC78.7.T6 | NLM WN 206 | DDC 616.07/54—dc23 LC record available at http://lccn.loc.gov/2016001268

Executive Content Strategist: Robin Carter
Senior Content Development Specialist: Ann Ruzycka Anderson
Publishing Services Manager: Patricia Tannian
Senior Project Manager: Cindy Thoms
Design Direction: Amy Buxton

Printed in China

Last digit is the print number: 9 8 7 6 5 4 3 2 1

This book is dedicated to Elizabeth E. Haaga, daughter of John and Ellen Haaga, who was born on August 19, 1972, and died December 9, 1985. Beth had a disseminated neuroblastoma, which was diagnosed in 1984. She was treated with a bone marrow transplant and died from graft-versus-host disease and infection. As her parents, we loved her dearly and cherish the memory of her early years when she was well. After the onset of her illness, we came to know that her gentle and loving nature was accompanied by a remarkably strong character. She endured her pain and suffering without bitterness and never sought to hurt those who loved her. Indeed, most incredulously, she tried to lessen our emotional pain even while enduring her physical discomforts. Many authors have marveled at the qualities of children, and although Beth's short life and premature death have left us saddened beyond comprehension, her remarkable courage and sweetness have given us a lasting pride and respect. We remember her lovingly.

The book is also dedicated to my wonderful family: my wife and soul mate, Ellen, and our children, Matthew and Stacie Haaga, Timothy and Molly Haaga, and Rebecca Haaga. Although professional successes are important and rewarding, the joy and pride of a loving family far surpass such accomplishments. All my love to my current family (and any future additions).

John R. Haaga

I am proud that my efforts as a "narrative diagnostician" have helped young physicians familiarize themselves with the challenges of modern clinical radiology. Hence, professionally, I want to dedicate this book to the wonderful mentors with whom I was honored to work over the years. A hallmark of any medical science is its continuously evolving and expanding knowledge base which, in turn, requires regular reevaluation and revitalization of established workflows. I want to thank my mentors for never tiring in reminding me of this fact and inspiring me to find new approaches to improve patient care.

Jonathan S. Lewin, MD (Emory University, Atlanta, GA), a gentleman scholar who guided me through the continuously evolving field of applied MRI physics and the parallel research methods; as a role model he influenced me greatly as I evolved into a scientist and mentor myself.

Jeffrey L. Duerk, PhD (Case Western Reserve University, Cleveland, OH), an exceptional teacher and visionary inventor, never tiring of "translating" formulas, figures, and (magnetic) field theories, thereby bringing together physicists and physicians in order to broaden everyone's horizon beyond expectation.

Erik K. Paulson, MD (Duke University Medical Center, Durham, NC), an outstanding diagnostician, teacher and leader who inspired me not only with his expertise and devotion to medical science and clinical practice but also through his willingness to explore unbeaten paths, thereby assembling an outstanding group of like-minded physicians and clinicians who cross-inspire each other.

And finally, my life-long friend, visionary academician and exceptional mentor, Elmar M. Merkle, MD (University Hospital of Basel, Basel, Switzerland), who has been there every step of the way and without whom my career would not have been possible.

When we all met initially, we all were in young stages of our careers. Over the evolving decades, our friendships formed and matured, emphasizing this most important characteristic of mentorship. Even now, meeting together with the now Executive Vice President for Health Affairs, the Dean of Biomedical Engineering, and two Chairmen of visionary and fascinating radiology departments, respectively, helpful and honest advice is always obtained, for mentorship is seen by these outstanding individuals as a lifelong responsibility. Thank you to all.

I also want to dedicate this book to my parents, brother, and wife, who, without having (too much of) a choice, have been there every step of the way and always encouraged me to live a life as a Weltbürger, finding friends and mentors all across the world. I will see you at home, wherever this will be; thank you for everything.

Daniel T. Boll

SECTION EDITORS

Kristine A. Blackham, MD
Assistant Professor
Divisions of Radiology and Neurosurgery
University Hospitals/Case Medical Center
Case Western Reserve University School of Medicine
Cleveland, Ohio

Mauricio Castillo, MD
Distinguished Professor of Radiology
Chief of Neuroradiology
University of North Carolina
Chapel Hill, North Carolina

Thorsten R. Fleiter, MD
Associate Professor
Department of Diagnostic Imaging and Nuclear Medicine
University of Maryland Medical Center
R Adams Cowley Shock Trauma Center
Baltimore, Maryland

Robert C. Gilkeson, MD
Director of Cardiothoracic Imaging
Professor of Radiology
University Hospitals/Case Medical Center
Case Western Reserve University School of Medicine
Cleveland, Ohio

Claudia M. Hillenbrand, PhD
Associate Member
Department of Diagnostic Imaging
Division of Translational Imaging Research
St. Jude Children's Research Hospital
Memphis, Tennessee

Richard A. Leder, MD
Associate Professor of Radiology
Clinical Associate in Surgery
Duke University School of Medicine
Durham, North Carolina

Jeong Min Lee, MD
Professor
Department of Radiology
Seoul National University Hospital
Seoul, Korea

Suresh K. Mukherji, MD, MBA, FACR
Professor and Chairman
Department of Radiology
Walter F. Patenge Endowed Chair
Chief Medical Officer and Director of Health Care Delivery
Michigan State University Health Team
East Lansing, Michigan

Raj M. Paspulati, MD
Associate Professor
Department of Radiology
University Hospitals/Case Medical Center
Case Western Reserve University School of Medicine
Cleveland, Ohio

Prabhakar Rajiah, MD
Associate Professor of Radiology
Cardiothoracic Imaging
Associate Director of Cardiac CT and MRI
University of Texas Southwestern Medical Center
Dallas, Texas

Mark R. Robbin, MD
Professor
Department of Radiology
Chief, Musculoskeletal Imaging
University Hospitals/Case Medical Center
Case Western Reserve University School of Medicine
Cleveland, Ohio

Ehsan Samei, PhD, DABR, FAAPM, FSPIE
Professor of Radiology, Medical Physics, Biomedical Engineering, Physics, and Electrical and Computer Engineering
Director, Carl E. Ravin Advanced Imaging Laboratories
Founding Chief
Clinical Imaging Physics Group
Duke University Medical Center
Durham, North Carolina

Jeffrey L. Sunshine, MD, PhD
Professor of Radiology, Neurology, Neurosurgery
Vice Chairman, Department of Radiology
University Hospitals/Case Medical Center
Case Western Reserve University School of Medicine
Chief Medical Information Officer, University Hospitals
Cleveland, Ohio

Frank K. Wacker, MD
Institute of Diagnostic and Interventional Radiology
University School of Medicine
Hannover, Germany

CONTRIBUTORS

James J. Abrahams, MD
Professor, Diagnostic Radiology
Diagnostic Radiology Program
Fellowship Director, Neuroradiology
Yale University School of Medicine
New Haven, Connecticut
Orbit

Michael Abrahams, MD
Department of Emergency Medicine
University of Toledo
Toledo, Ohio
Orbit

Federica Agosta, MD, PhD
Neuroimaging Research Unit
Institute of Experimental Neurology
Division of Neuroscience
San Raffaele Scientific Institute
Vita-Salute San Raffaele University
Milan, Italy
Neurodegenerative Disorders

Muneeb Ahmed, MD, FSIR
Chief
Division of Vascular and Interventional Radiology
Beth Israel Deaconess Medical Center
Associate Professor of Radiology
Harvard Medical School
Boston, Massachusetts
Image-Guided Ablation of Parenchymal Organs

Supreeta Arya, MD, DMRD, DNB
Professor
Radiodiagnosis
Tata Memorial Hospital
Mumbai, India
Pharynx

Yong Ho Auh, MD
Professor of Radiology
Weill Cornell Medical College of Cornell University
Attending Radiologist
New York-Presbyterian Hospital
New York, New York
Mesentery

Romulo Baltazar, MD
Attending Radiologist
Imaging Subspecialists of North Jersey
St. Joseph's Regional Medical Center
Paterson, New Jersey
Knee

Mustafa R. Bashir, MD
Assistant Professor
Department of Radiology
Duke University Medical Center
Durham, North Carolina
Tissue Characterization in Liver Imaging Using Advanced MR Techniques

Javier Beltran, MD, FACR
Chairman
Department of Radiology
Maimonides Medical Center
Brooklyn, New York
Clinical Director of Musculoskeletal Radiology
Radisphere National Radiology Group
Beachwood, Ohio
Knee

Stuart Bentley-Hibbert, MD, PhD
Associate Professor of Radiology
Department of Radiology
Columbia University Medical Center
New York, New York
Mesentery

Shweta Bhatt, MD
Associate Professor
Department of Imaging Sciences
University of Rochester
Rochester, New York
Kidney

Nicholas Bhojwani, MD
Department of Radiology
University Hospitals/Case Medical Center
Cleveland, Ohio
Knee
Musculoskeletal Tumors

Sotirios Bisdas, MD, PhD, MSc
Neuroradiology Consultant
National Hospital for Neurology and Neurosurgery
Honorary Senior Lecturer
University College London
London, United Kingdom
Professor of Radiology
Department of Neuroradiology
Karls Eberhard University
Tübingen, Germany
Adenopathy and Neck Masses

Kristine A. Blackham, MD
Assistant Professor
Divisions of Radiology and Neurosurgery
University Hospitals/Case Medical Center
Case Western Reserve University
Cleveland, Ohio
Intracranial Neoplasms

Donna G. Blankenbaker, MD
Professor of Radiology
Department of Radiology
University of Wisconsin School of Medicine and Public Health
Madison, Wisconsin
Hip and Pelvis

Uttam K. Bodanapally, MBBS
Assistant Professor
Department of Diagnostic Radiology and Nuclear Medicine
University of Maryland Medical Center
R Adams Cowley Shock Trauma Center
Baltimore, Maryland
Traumatic Brain Injury

Phillip M. Boiselle, MD
Professor of Radiology
Associate Dean for Academic and Clinical Affairs
Harvard Medical School
Boston, Massachusetts
Airway

Daniel T. Boll, MD, FSCBT
Professor of Radiology
Section Chief Abdominal and Oncologic Imaging
University Hospital of Basel
Basel, Switzerland
Liver: Normal Anatomy, Imaging Techniques, and Diffuse Diseases
Tissue Characterization in Liver Imaging Using Advanced Magnetic Resonance Techniques

Eliana Bonfante, MD
Assistant Professor of Radiology
Department of Diagnostic and Interventional Imaging
University of Texas Health Science Center
Houston, Texas
Spinal Trauma

Jeffrey R. Brace, MD
Assistant Professor of Radiology
University of Minnesota Medical Center, Fairview
Hennepin County Medical Center
Minneapolis Veterans Affairs Medical Center
Minneapolis, Minnesota
Intracranial Neoplasms

Miriam A. Bredella, MD
Associate Professor of Radiology
Harvard Medical School
Department of Radiology
Musculoskeletal Imaging and Interventions
Massachusetts General Hospital
Boston, Massachusetts
Shoulder

Michael K. Brooks, MD, MPH
Clinical Assistant Professor of Radiology
SUNY-Stony Brook
Department of Radiology
Division of Musculoskeletal Imaging and Intervention
Winthrop University Hospital
Mineola, New York
Degenerative Disease

Christopher Brown, MD
Research Analyst
Department of Diagnostic Radiology
University of Maryland Medical Center
Baltimore, Maryland
Coronary Arteries, Heart, and Pericardium

Ji Y. Buethe, MD
Chief Resident
Department of Radiology
University Hospitals/Case Medical Center
Cleveland, Ohio
Image-Guided Drainages

John A. Carrino, MD, MPH
Vice Chairman of Radiology
Department of Radiology and Imaging
Hospital for Special Surgery
New York, New York
High-Resolution 3T Magnetic Resonance Neurography: Applications, Techniques, and Pitfalls

Francesca Caso, MD
Neuroimaging Research Unit
Institute of Experimental Neurology
Division of Neuroscience
San Raffaele Scientific Institute
Vita-Salute San Raffaele University
Milan, Italy
Neurodegenerative Disorders

Mauricio Castillo, MD
Distinguished Professor of Radiology
Chief of Neuroradiology
University of North Carolina
Chapel Hill, North Carolina
Brain Proton Magnetic Resonance Spectroscopy
Cystic Lesions

Onofrio Catalano, MD
Assistant Professor of Radiology
Division of Abdominal Surgery
Harvard Medical School
Boston, Massachusetts
Pancreas

Majid Chalian, MD
Radiology House Staff, PGY3
Radiology
University Hospitals
Case Western Reserve University
Cleveland, Ohio
High Resolution 3T Magnetic Resonance Neurography: Applications, Techniques, Pitfalls

Ronil V. Chandra, MBBS (Hons), MMed, FRANZCR
Associate Professor
Neuroradiology Service
Monash Imaging
Monash Health Stroke and Ageing Research Centre
Monash University
Melbourne, Victoria, Australia
Stroke

Tushar Chandra, MD
Clinical Instructor
Radiology
Medical College of Wisconsin
Milwaukee, Wisconsin
Pharynx

Apeksha Chaturvedi, MD
Assistant Professor
Radiology
University of Rochester Medical Center
Rochester, New York
Chest Imaging in the Pediatric Patient

Avneesh Chhabra, MD
Department of Radiology
University of Texas Southwestern Medical Center
Dallas, Texas
High-Resolution 3T Magnetic Resonance Neurography: Applications, Techniques, and Pitfalls

Dong-il Choi, MD
Associate Professor
Sungkyunkwan University School of Medicine
Faculty, Department of Radiology
Samsung Medical Center
Seoul, Republic of Korea
Biliary Tract and Gallbladder

Jared D. Christensen, MD
Assistant Professor
Radiology
Duke University Medical Center
Durham, North Carolina
Mediastinal Disease

Michael Coffey, MD
Assistant Professor
Radiology
Case Western Reserve University School of Medicine
Cleveland, Ohio
Demyelinating Disease and Leukoencephalopathies

Brian Cox, MD
Department of Radiology
University of Texas Southwestern Medical Center
Dallas, Texas
High-Resolution 3T Magnetic Resonance Neurography: Applications, Techniques, and Pitfalls

Kelly L. Cox, DO
Assistant Professor
Radiology and Imaging Sciences
Emory University Hospitals and School of Medicine
Atlanta, Georgia
Female Pelvis

Sheilah Curran-Melendez, MD
Department of Diagnostic Radiology
Allegheny General Hospital
Pittsburgh, Pennsylvania
Meningeal Processes

Hugh D. Curtin, MD
Professor of Radiology
Harvard Medical School
Chief of Radiology
Massachusetts Eye and Ear
Boston, Massachusetts
Larynx

Carlo N. De Cecco, MD, PhD
Assistant Professor
Department of Radiology and Radiological Sciences
Division of Cardiovascular Imaging
Medical University of South Carolina
Charleston, South Carolina
Advanced Cardiovascular CT Imaging

Alfred Delumpa, MD
Fellow
Department of Neuroradiology
Baylor College of Medicine
Houston, Texas
Spinal Tumors

David R. Di Lorenzo, MD
Diagnostic Radiology
University Hospitals/Case Medical Center
Cleveland, Ohio
Peritoneum

Vikram S. Dogra, MD
Professor of Radiology and Urology
Department of Imaging Sciences
University of Rochester
Rochester, New York
Kidney

David Dreizin, MD
Assistant Professor
Department of Diagnostic Radiology and Nuclear Medicine
University of Maryand Medical Center
R Adams Cowley Shock Trauma Center
Baltimore, Maryland
Spinal Cord Injury
Traumatic Brain Injury

Jeremy J. Erasmus, MBBCh
Professor
Diagnostic Radiology
University of Texas MD Anderson Cancer Center
Houston, Texas
Neoplastic Disease of the Lung

Maryam Etesami, MD
Radiology
Case Western Reserve University
University Hospitals Case Medical Center
Cleveland, Ohio
Chest Imaging in the Pediatric Patient

Steven Falcone, MD, MBA
Professor
Radiology, Neurological Surgery, Ophthalmology
Executive Dean for Clinical Affairs
Miller School of Medicine
Chief Executive Officer
University of Miami Medical Group
Associate Vice President for Medical Affairs
University of Miami
Miami, Florida
Systemic Diseases Affecting the Spine

Massimo Filippi, MD
Professor
Neuroimaging Research Unit
Department of Neurology
Division of Neuroscience
Institute of Experimental Neurology
San Raffaele Scientific Institute
Vita-Salute San Raffaele University
Milan, Italy
Neurodegenerative Disorders

Thorsten R. Fleiter, MD
Associate Professor
Department of Diagnostic Imaging and Nuclear Medicine
University of Maryland Medical Center
R Adams Cowley Shock Trauma Center
Baltimore, Maryland
Traumatic Brain Injury

Tomás Franquet, MD
Chief, Section of Thoracic Imaging
Radiology
Hospital de Sant Pau
Associate Professor of Radiology
Universitat Autonoma de Barcelona
Barcelona, Spain
Nonneoplastic Parenchymal Lung Disease

Melanie B. Fukui, MD
Aurora Neuroscience Innovation Institute
St. Luke's Medical Center
Milwaukee, Wisconsin
Meningeal Processes

Stephen R. Fuller, BS
Department of Radiology and Radiological Sciences
Division of Cardiovascular Imaging
Medical University of South Carolina
Charleston, South Carolina
Advanced Cardiovascular CT Imaging

Nicholas L. Fulton, MD
Resident
Radiology
University Hospitals/Case Medical Center
University Heights, Ohio
Vasculogenesis

Romyll Garcia, MD
Voluntary Assistant Professor
Radiology
University of Miami
Miami, Florida
Systemic Diseases Affecting the Spine

Amilcare Gentili, MD
Professor
Radiology
University of California–San Diego
San Diego, California
Musculoskeletal Tumors

Ritu R. Gill, MD, MPH
Associate Radiologist
Assistant Professor of Radiology
Brigham and Women's Hospital
Harvard Medical School
Boston, Massachusetts
Disease of the Pleura, Chest Wall, and Diaphragm

John L. Go, MD
Director of Head and Neck Imaging
Medical Director of the Imaging Science Center
University of Southern California
Keck School of Medicine
Los Angeles, California
Cerebral Infections and Inflammation

Joseph R. Grajo, MD
Assistant Professor of Radiology
University of Florida College of Medicine
Gainesville, Florida
Male Pelvis

Sachin K. Gujar, MBBS, MD
Assistant Professor
Neuroradiology Division
Russell H. Morgan Department of Radiology and Radiological Science
Johns Hopkins University School of Medicine
Baltimore, Maryland
Functional Magnetic Resonance Imaging

Junyu Guo, PhD
MR Scientist
Diagnostic Imaging
St. Jude Children's Research Hospital
Memphis, Tennessee
Contrast-Enhanced Magnetic Resonance Imaging

Amit Gupta, MD
Fellow, Neuroradiology
University Hospitals/Case Medical Center
Cleveland, Ohio
Demyelinating Disease and Leukoencephalopathies

Hyun Kwon Ha, MD
Professor of Radiology
University of Ulsan College of Medicine
Professor and Chief of Gastrointestinal Section
Department of Radiology
Asan Medical Center
Seoul, Republic of Korea
Gastrointestinal Tract

John R. Haaga, MD, FACR, FSIR, FSCBT, FSRS
Gold Medalist AARS and SCBTMRI
Professor of Radiology
Case Western Reserve University School of Medicine
Emeritus Chairman and Professor of Radiology
University Hospitals/Case Medical Center
Case Western Reserve University School of Medicine
Cleveland, Ohio
Image-Guided Aspirations and Biopsies
Imaging Principles in Computed Tomography
Peritoneum
Vasculogenesis

Timothy L. Haaga, MD
Clinical Assistant Professor
Radiology
University Hospitals/Case Medical Center
Case Western Reserve University School of Medicine
Cleveland, Ohio
Image-Guided Aspirations and Biopsies

Mukesh G. Harisinghani, MD
Professor of Radiology
Harvard Medical School
Boston, Massachusetts
Male Pelvis

Tobias Heye, MD
Department of Radiology
University Hospital of Basel
Basel, Switzerland
Tissue Characterization in Liver Imaging Using Advanced Magnetic Resonance Techniques

Claudia M. Hillenbrand, PhD
Associate Member
Department of Diagnostic Imaging
Division of Translational Imaging Research
St. Jude Children's Research Hospital
Adjunct Associate Professor
Department of Biomedical Engineering
University of Memphis
Memphis, Tennessee
Magnetic Resonance Imaging in the Pediatric Patient

Lisa M. Ho, MD
Associate Professor of Radiology
Department of Radiology
Duke University Medical Center
Durham, North Carolina
Adrenal Glands

Ellen Hoeffner, MD
Professor of Radiology
University of Michigan
Ann Arbor, Michigan
Pharynx
Temporal Bone

Alena Horská, PhD
Assistant Professor
Russell H. Morgan Department of Radiology and Radiological Science
Division of Neuroradiology
Johns Hopkins University School of Medicine
Baltimore, Maryland
Brain Proton Magnetic Resonance Spectroscopy

David W. Jordan, PhD
Senior Medical Physicist, Radiology
University Hospitals/Case Medical Center
Assistant Professor, Radiology
Case Western Reserve University
Cleveland, Ohio
Imaging Principles in Computed Tomography
Imaging Principles in Magnetic Resonance Imaging

Varsha Joshi, DNB, DMRD
Senior Consultant
Division of CT and MRI
Vijaya Diagnostic Centres
Hyderabad, India
Visiting Consultant
Tata Medical Center
Kolkata, India
Paranasal Sinuses

Sue C. Kaste, DO
Full Member
Department of Diagnostic Imaging
Department of Oncology
St. Jude Children's Research Hospital
Full Professor, Radiology
University of Tennessee
School of Health Sciences
Memphis, Tennessee
Magnetic Resonance Imaging in the Pediatric Patient

Simon Rupe Khangure, MD, MBBS, BMdSc, FRANZCR
Neuroradiology Service
Monash Imaging
Monash Health
Melbourne, Victoria, Australia
Stroke

Stephen A. Kieffer, MD
Professor of Radiology (Neuroradiology)
University of Minnesota Medical School
Attending Radiologist
University of Minnesota Medical Center, Fairview
Hemepin County Medical Center
Minneapolis Veterans Affairs Medical Center
Minneapolis, Minnesota
Intracranial Neoplasms

Ah Young Kim, PhD
Associate Professor of Radiology
University of Ulsan College of Medicine
Associate Professor of Radiology
Division of Abdominal Radiology
Asan Medical Center
Seoul, Republic of Korea
Gastrointestinal Tract

Jung Hoon Kim, MD
Assistant Professor
Medicine-Geriatrics
Baylor College of Medicine
Houston, Texas
Mesentery

Kyoung Won Kim, MD, PhD
Assistant Professor of Radiology
University of Ulsan College of Medicine
Faculty Member, Department of Radiology
Asan Medical Center
Seoul, Republic of Korea
Biliary Tract and Gallbladder

Paul E. Kim, MD
University of Southern California
Keck School of Medicine
Los Angeles, California
Cerebral Infections and Inflammation

Seth Kligerman, MD
Associate Professor of Radiology
Diagnostic Radiology and Nuclear Medicine
University of Maryland
Baltimore, Maryland
Coronary Arteries, Heart, and Pericardium

Satoshi Kobayashi, MD, PhD
Professor
Quantum Medical Technology
Kanazawa University Graduate School of Medical Science
Kanazawa, Japan
Liver: Focal Hepatic Mass Lesions

Christos Kosmas, MD
Assistant Professor of Radiology
Division of Musculoskeletal Imaging
University Hospitals/Case Medical Center
Case Western Reserve University
Cleveland, Ohio
Foot and Ankle

Gerdien Kramer, MD
Department of Thoracic Imaging
Hopital Calmette
Universite Lille Nord de France
Lille, France
Coronary Arteries, Heart, and Pericardium

Timo Krings, MD, PhD, FRCPC
The David Braley and Nancy Gordon Chair in Interventional Neuroradiology
Chief of Diagnostic and Interventional Neuroradiology
Toronto Western Hospital and University Health Network
Professor of Radiology and Surgery
University of Toronto
Toronto, Ontario, Canada
Vascular Lesions

Lester Kwock, PhD
Professor of Radiology
University of North Carolina School of Medicine
Chapel Hill, North Carolina
Brain Proton Magnetic Resonance Spectroscopy

Theodore C. Larson III, MD
Director of Neurointervention
Centura Neurosciences
St. Anthony Hospital
Lakewood, Colorado
Cerebral Aneurysms and Cerebrovascular Malformations

Leslie K. Lee, MD
Instructor in Radiology
Harvard Medical School
Boston, Massachusetts
Male Pelvis

Seung Soo Lee, MD
Assistant Professor of Radiology
University of Ulsan College of Medicine
Seoul, Republic of Korea
Gastrointestinal Tract

Young-Jun Lee, MD, PhD
Associate Professor, Radiology
Hanyang University Hospital
Seoul, South Korea
Spinal Vascular Diseases

Alexander Lerner, MD
Assistant Professor of Clinical Radiology
Radiology
University of Southern California
Keck School of Medicine
Los Angeles, California
Cerebral Infections and Inflammation

Jae Hoon Lim, MD
Department of Radiology
Myongji Hospital
Goyang, Republic of Korea
Biliary Tract and Gallbladder

Chia-Shang J. Liu, MD, PhD
Assistant Professor
Radiology
University of Southern California
Keck School of Medicine
Los Angeles, California
Cerebral Infections and Inflammation

Minh Lu, MD
Radiology
University of Maryland
Baltimore, Maryland
Coronary Arteries, Heart, and Pericardium

Kenneth Lury, MD
Assistant Professor (Retired)
Radiology
University of North Carolina
Chapel Hill, North Carolina
Noninfectious Inflammatory Diseases Affecting the Spinal Cord

Calvin T. Ma, MD
Staff Radiologist
Sutter Imaging
Sutter Health Sacramento Sierra Region
Sacramento, California
Knee

Henry Ma, MBBS, FRACP
Associate Professor
Stroke Unit, Monash Health
Stroke and Ageing Research Centre
Monash University
Melbourne, Victoria, Australia
Stroke

Bahar Mansoori, MD
Department of Radiology
University Hospitals
Case Western Reserve University
Cleveland, Ohio
High-Resolution 3T Magnetic Resonance Neurography: Applications, Techniques, and Pitfalls

Daniel Mascarenhas, BS
Department of Diagnostic Radiology and Nuclear Medicine
University of Maryland Medical Center
R Adams Cowley Shock Trauma Center
Baltimore, Maryland
Spinal Cord Injury
Traumatic Brain Injury

Osamu Matsui, MD, PhD
Professor Emeritus Radiology
Kanazawa University Graduate School of Medical Science
Kanazawa, Japan
Liver: Focal Hepatic Mass Lesions

Joseph P. Mazzie, DO
Clinical Assistant Professor of Radiology
SUNY-Stony Brook
Department of Radiology
Division of Musculoskeletal Imaging and Intervention
Winthrop University Hospital
Mineola, New York
Degenerative Disease

H. Page McAdams, MD
Professor of Radiology
Radiology
Duke University Medical Center
Durham, North Carolina
Mediastinal Disease

Indu Rekha Meesa, MD, MS
Neuroradiology and Pediatric Radiologist
Summit Radiology
Fort Wayne, Indiana
Neuroradiology and Pediatric Radiology Fellow
Department of Radiology
University of Michigan
Ann Arbor, Michigan
Imaging of the Head and Neck in the Pediatric Patient

Carolyn Cidis Meltzer, MD
William P. Timmie Professor and Chair
Department of Radiology and Imaging Sciences
Associate Dean for Research
Emory University School of Medicine
Atlanta, Georgia
Meningeal Processes

Elmar M. Merkle, MD
Department of Radiology
University Hospital of Basel
Basel, Switzerland
Tissue Characterization in Liver Imaging Using Advanced MR Techniques

Achille Mileto, MD
Department of Radiology
Duke University School of Medicine
Durham, North Carolina
Liver: Normal Anatomy, Imaging Techniques, and Diffuse Diseases

Suyash Mohan, MD, PDCC
Assistant Professor of Radiology
Radiology, Neuroradiology Division
University of Pennsylvania
Philadelphia, Pennsylvania
Pharynx
Temporal Bone

Jesse Montagnese, MD
Assistant Professor
Radiology
University of Pittsburgh
Pittsburgh, Pennsylvania
Intracranial Neoplasms

Sameh K. Morcos, FRCS, FFRRCSI, FRCR
Professor of Diagnostic Imaging
University of Sheffield
Consultant Radiologist
Northern General Hospital
Sheffield, United Kingdom
Contrast Nephropathy and Its Management

Fanny E. Morón, MD
Associate Professor of Diagnostic Radiology
Baylor College of Medicine
Houston, Texas
Spinal Neoplasms

Suresh Mukherji, MD, MBA, FACR
Professor and Chairman
Department of Radiology
Walter F. Patenge Endowed Chair
Chief, Medical Officer and Director of Health Care Delivery
Michigan State University Health Team
East Lansing, Michigan
Imaging of the Head and Neck in the Pediatric Patient

Dean A. Nakamoto, MD
Section Chief, Abdominal Imaging
Radiology
University Hospitals/Case Medical Center
Cleveland, Ohio
Computed Tomography—Guided Drainage
Spleen

Sadhna B. Nandwana, MD
Assistant Professor
Department of Radiology and Imaging Sciences
Emory University Hospitals and School of Medicine
Atlanta, Georgia
Female Pelvis

John P. Nazarian, MD
Resident, Radiology
University Hospitals/Case Medical Center
Cleveland, Ohio
Demyelinating Disease and Leukoencephalopathies

Manal Nicolas-Jilwan, MD
Radiology
University of Virginia Health System
Charlottesville, Virginia
Congenital Abnormalities

Sherif G. Nour, MD, FRCR
Director, Interventional MRI Program
Associate Professor of Radiology and Imaging Sciences
Department of Radiology and Imaging Sciences
Emory University Hospitals and School of Medicine
Atlanta, Georgia
Female Pelvis
MRI-Guided Interventions

A. Orlando Ortiz, MD, MBA, FACR
Clinical Professor of Radiology
SUNY-Stony Brook
Chairman, Department of Radiology
Winthrop University Hospital
Mineola, New York
Degenerative Disease

Theeraphol Panyaping, MD
Diagnostic Neuroradiology Division
Department of Radiology
Ramathibodi Hospital
Mahidol University
Ratchathewi, Bangkok, Thailand
Spinal Infection

Seong Ho Park, MD
Associate Professor of Radiology
University of Ulsan College of Medicine
Asan Medical Center
Seoul, Republic of Korea
Gastrointestinal Tract

Raj M. Paspulati, MD
Associate Professor
Radiology
University Hospitals/Case Medical Center
Case Western Reserve University
Cleveland, Ohio
Liver Transplantation
Rectum

Manuel Patino, MD
Postdoctoral Fellow
Division of Abdominal Imaging
Massachusetts General Hospital
Boston, Massachusetts
Pancreas

Thanh Phan, MD, MBBS, FRACP
Professor
Stroke Unit, Monash Health
Stroke and Ageing Research Centre
Monash University
Melbourne, Australia
Stroke

Jay J. Pillai, MD
Director of Functional MRI
Associate Professor
Neuroradiology Division
Russell H. Morgan Department of Radiology and Radiological Science
Johns Hopkins University School of Medicine
Baltimore, Maryland
Brain Proton Magnetic Resonance Spectroscopy
Functional Magnetic Resonance Imaging

Colin S. Poon, MD, PhD, FRCPC
Assistant Clinical Professor
Department of Diagnostic Radiology
Yale University School of Medicine
New Haven, Connecticut
Staff Radiologist
Orillia Soldiers' Memorial Hospital
Orillia, Ontario, Canada
Orbit

Andrea Prochowski, MD
Postdoctoral Fellow
Division of Abdominal Imaging
Massachusetts General Hospital
Boston, Massachusetts
Pancreas

Anandh Rajamohan, MD
Assistant Professor
Radiology
University of Southern California
Keck School of Medicine
Los Angeles, California
Cerebral Infections and Inflammation

Prabhakar Rajiah, MD
Associate Professor of Radiology
Cardiothoracic Imaging
Associate Director of Cardiac CT and MRI
University of Texas Southwestern Medical Center
Dallas, Texas
Chest Imaging in the Pediatric Patient

Parvati Ramchandani, MD
Professor of Radiology and Surgery, Section Chief GU Radiology
Department of Radiology
Hospital of the University of Pennsylvania
Philadelphia, Pennsylvania
Retroperitoneum

Wilburn E. Reddick, PhD
Member Faculty
Diagnostic Imaging
St. Jude Children's Research Hospital,
Memphis, Tennessee
Contrast-Enhanced Magnetic Resonance Imaging

Matthias Renker, MD
Visiting Scholar
Department of Radiology and Radiological Services
Division of Cardiovascular Imaging
Medical University of South Carolina
Charleston, South Carolina
Resident, Department of Medicine I, Cardiology/Angiology
University Hospital Giessen
Giessen, Germany
Advanced Cardiovascular CT Imaging

Roy Riascos, MD, DABR
Associate Professor
Chief of Neuroradiology
Department of Diagnostic and Interventional Imaging
University of Texas Health Science Center at Houston
Houston, Texas
Spinal Trauma

Mark R. Robbin, MD
Professor
Department of Radiology
Chief, Division of Musculoskeletal Imaging
University Hospitals/Case Medical Center
Case Western Reserve School of Medicine
Cleveland, Ohio
Musculoskeletal Tumors

Santiago E. Rossi, MD
Centro de Diagnostico Dr Enrique Rossi
Buenos Aires, Argentina
Neoplastic Disease of the Lung

Dushyant Sahani, MD
Associate Professor of Radiology
Harvard Medical School
Director of Computed Tomography
Massachusetts General Hospital
Division of Abdominal Imaging and Intervention
Boston, Massachusetts
Pancreas

Nisha Sainani, MD
Assistant Professor of Radiology
Harvard Medical School
Staff Radiologist
Abdominal Imaging and Intervention
Brigham and Women's Hospital
Boston, Massachusetts
Pancreas

Haris I. Sair, MD
Assistant Professor
Neuroradiology Division
Russell H. Morgan Department of Radiology and Radiological Science
Johns Hopkins University School of Medicine
Baltimore, Maryland
Functional Magnetic Resonance Imaging

Dilan Samarawickrama, MD
Neuroradiology Fellow
Radiology
University of Michigan
Ann Arbor, Michigan
Temporal Bone

Rima Sansi, DNB
Clinical Associate
Department of Radiology
Sir H.N. Reliance Foundation Hospital and Research Centre
Prarthana Samaj, Girgaum, Mumbai, India
Paranasal Sinuses

Asha Sarma, MD
Resident
Radiology
Brigham and Women's Hospital
Boston, Massachusetts
Disease of the Pleura, Chest Wall, and Diaphragm

Piyush Saxena, DNB, MBBS
Consultant Radiologist and Chief of MRI
Radiodiagnosis
Vishesh Hospital and Diagnostics
Indore, Madhya Pradesh, India
Paranasal Sinuses

U. Joseph Schoepf, MD
Professor
Department of Radiology and Radiological Sciences
Division of Cardiovascular Imaging
Director, CT Research and Development
Medical University of South Carolina
Charleston, South Carolina
Advanced Cardiovascular CT Imaging

Eric Schrauben, PhD
Medical Physics
University of Wisconsin–Madison
Madison, Wisconsin
Imaging Principles in Magnetic Resonance Angiography

Ken L. Schreibman, MD, PhD
Professor of Radiology
Division of Musculoskeletal Imaging
University of Wisconsin–Madison
University of Wisconsin Hospitals and Clinics
Madison, Wisconsin
Foot and Ankle

Danielle M. Seaman, MD
Staff Radiologist
Radiology
Durham Veterans Affairs Medical Center
Durham, North Carolina
Mediastinal Disease

Nicole Seiberlich, PhD
Assistant Professor
Biomedical Engineering
Case Western Reserve University
Cleveland, Ohio
Imaging Principles in Magnetic Resonance Imaging

Saugata Sen, MD
Senior Consultant
Radiology and Nuclear Medicine
Tata Medical Center
Kolkata, West Bengal, India
Paranasal Sinuses

Rickin Shah, MD
Department of Radiology
University of Michigan Health System
Ann Arbor, Michigan
Temporal Bone

Steven Shankman, MD
Vice-Chairman, Department of Radiology
Maimonides Medical Center
Brooklyn, New York
Knee

Kenneth Sheah, MBBS FRCR MMed (Diagnostic Radiology)
Consultant Radiologist
Lifescan Imaging Pte Ltd
Singapore
Shoulder

Haojun Shi, MD
Assistant Professor of Radiology
Huazhong University of Science and Technology
Department of Radiology
Union Hospital
Wuhan, Hubei Province, China
Normal Anatomy

George Shih, MD
Adjunct Assistant Professor of Radiology
Columbia University College of Physicians and Surgeons
Associate Attending Radiologist
New York-Presbyterian Hospital
Associate Professor of Clinical Radiology
Weill Cornell Medical College
New York, New York
Mesentery

Mark S. Shiroishi, MD
Assistant Professor
Radiology
University of Southern California
Keck School of Medicine
Los Angeles, California
Cerebral Infections and Inflammation

Stephanie Soriano, MD
Radiology
University Hospitals/Case Medical Center
Cleveland, Ohio
Spleen

Cathy Soufan, MD
Neuroradiology Service
Monash Imaging
Monash Health
Melbourne, Victoria, Australia
Stroke

Jason W. Stephenson, MD
Assistant Professor of Radiology
Department of Radiology
University of Wisconsin School of Medicine and Public Health
Madison, Wisconsin
Hip and Pelvis

Stephen L. Stuckey, MBBS, MD, MMed, FRANZCR, FAANMS, PGDA
Director
Monash Imaging
Monash Health
Department of Imaging
Monash University
Melbourne, Victoria, Australia
Stroke

Mark Patrick Supanich, PhD
Associate Professor
Diagnostic Radiology and Nuclear Medicine
Rush University Medical Center
Chicago, Illinois
Computed Tomography Imaging Operation

Katarina Surlan-Popovic, MD, PhD
Associate Professor of Radiology
Clinical Institute of Radiology
University Medical Center Ljubljana
Ljubljana, Slovenia
Adenopathy and Neck Masses

Janio Szklaruk, PhD, MD
Professor of Diagnostic Radiology
University of Texas MD Anderson Cancer Center
Houston, Texas
Spinal Tumors

Gustavo A. Tedesqui, MD
Research Fellow
Neuroradiology
University of North Carolina
Chapel Hill, North Carolina
Cystic Lesions

Aaryani Tipirneni-Sajja, MS
Research Assistant
Division of Translational Imaging Research
Department of Diagnostic Imaging
St. Jude Children's Research Hospital
Research Assistant
Department of Biomedical Engineering
University of Memphis
Memphis, Tennessee
Magnetic Resonance Imaging in the Pediatric Patient

Drew A. Torigian, MD, MA
Associate Professor of Radiology
Department of Radiology
Hospital of the University of Pennsylvania
Philadelphia, Pennsylvania
Retroperitoneum

Erik M. Velez, MD
Department of Radiology
Beth Israel Deaconess Medical Center
Boston, Massachusetts
Image-Guided Ablation of Parenchymal Organs

Thomas J. Vogl, MD
Professor of Radiology
Chair
Department of Diagnostic and Interventional Radiology
University Hospital Frankfurt
Frankfurt, Germany
Adenopathy and Neck Masses

Charles S. White, MD
Professor of Radiology and Medicine
University of Maryland Medical Center
Baltimore, Maryland
Coronary Arteries, Heart, and Pericardium

Julian Lukas Wichmann, MD
Visiting Instructor
Department of Radiology and Radiological Sciences
Division of Cardiovascular Imaging
Medical University of South Carolina
Charleston, South Carolina
Resident
Department of Diagnostic and Interventional Radiology
University Hospital Frankfurt
Frankfurt, Germany
Advanced Cardiovascular CT Imaging

Oliver Wieben, PhD
Associate Professor
Medical Physics and Radiology
University of Wisconsin–Madison
Madison, Wisconsin
Imaging Principles in Magnetic Resonance Angiography

Leo Wolansky, MD
Professor, Radiology
Case Western Reserve University
School of Medicine
Cleveland, Ohio
Demyelinating Disease and Leukoencephalopathies

Hanping Wu, MD
Resident
Department of Radiology
University Hospitals/Case Medical Center
Cleveland, Ohio
Image-Guided Aspirations and Biopsies
Normal Anatomy

Haibo Xu, MD
Chairman
Department of Radiology
Zhongnan Hospital of Wuhan University
Wuhan, Hubei Province, China
Normal Anatomy

Chi-Shing Zee, MD
Professor of Radiology and Neurosurgery
Department of Radiology
Keck Hospital of University of Southern California
Los Angeles, California
Cerebral Infections and Inflammation

PREFACE

This sixth edition of *CT and MRI of the Whole Body* represents a monumental accomplishment for Elsevier and our many contributing authors, editors, and section editors who have contributed past and present. The authors of the current chapters are due many, many kudos because of the changes that have occurred in healthcare with the emphasis on "productivity" and RVUs. Institutions have reduced physician support in the form of secretaries, assistants, etc., which makes it very difficult for academic physicians to contribute to projects such as this book. THANK YOU, THANK YOU!

Being senior editor of this book has been a remarkable honor for me because it enabled me to collaborate with many radiologists and physicists. Everyone who has been involved for the past 40 years can take great pride in this book because it has formed the foundation for educating thousands of fellow radiologists in the United States and around the world. Over the years, radiologists from all over the world have expressed their gratitude for having this book available as a reference.

As I reflect back, I become nostalgic just thinking about how exciting radiology has been for the past 40 years. So many innovations and advances have been made. Of the contributions I have made, I am the most proud of developing CT interventions such as biopsies, abscess drainages, nerve blocks, the Topogram/Scoutview, and radiation dose reduction. It is very flattering that the Smithsonian Institution asked for and accepted for curation several personal artifacts related to these innovations.

Over the years I have met many pioneers in the field of imaging, but my two favorites were Sven Seldinger, MD (Fig. 1), and Paul Lauterbur, PhD (Fig. 2), as pictured below. Dr. Seldinger was a very dynamic person who developed the Seldinger Technique for angiography. Unfortunately, he didn't receive the recognition he deserved until late in his career. Few know that he did not receive an academic appointment until we awarded him with one at Case Western Reserve University. Paul Lauterbur was the genius who received the Nobel Prize for MRI. Strangely enough, he and I lived in the same small town, Troy, Ohio, for a number of years. His sense of humor as well as his science was of Nobel quality.

I have taken the editor's prerogative of referencing and publishing my own innovations in this book. My last innovation, which I am confident will improve the diagnosis and treatment of cancer, is the ALPHA concept, which is discussed in Chapter 70. The concept has been published in the journals *Surgery* and the *American Journal of Roentgenology* (AJR). We have just finished the experimental proof of ALPHA, which includes standard laboratory tests, but also the latest RNA sequencing tests. We will be submitting it for publication soon. This concept explains how aerobic metabolism has been overemphasized and that glycolysis is more important for the development and treatment of cancer.

I hope and believe that we will be able to diagnose and cure many more cancers with this knowledge. Readers are encouraged to search the literature for future publications by my protégés who are continuing this work. There are numerous young physicians working on this concept who have accomplished much to date. I would like to acknowledge a number of young investigators, Hooman Yarmohammadi, MD; Luke Wilkins, MD; Steven Dreyer, MD; Dan Patel, MD; Nicholas Fulton, and Ji Buethe, for their hard work and commitment to continue work on this ALPHA concept.

John R. Haaga

FIG 1 Sven Seldinger *(right)* and John R. Haaga.

FIG 2 Paul Lauterbur *(right)* and John R. Haaga.

PREFACE TO THE FIRST EDITION

Since the introduction of computed tomography (CT) in 1974, there has been a remarkable revolution in the medical treatment of patients. The clinical use of CT has had a broad positive impact on patient management. Literally thousands of patients have been saved or their quality of life improved as a result of the expeditious and accurate diagnosis provided by CT. This improvement in diagnosis and management has occurred in all medical subspecialties, including neurological, pulmonary, cardiac, gastrointestinal, genitourinary, and neuromuscular medicine. Aside from the imaging advantages provided, the role of CT in planning and performing interventional procedures is now recognized. It is the most accurate method for guiding procedures to obtain cytological, histological, or bacteriological specimens and for performing a variety of therapeutic procedures.

The evolution and refinement of CT equipment have been as remarkable as the development of patient diagnosis. When we wrote our first book on CT, the scanning unit used was a 2-minute translate-rotate system. At the time of our second book the 18-second translate-rotate scanning unit was in general use. Currently standard units in radiological practice are third and fourth generation scanners with scan times of less than 5 seconds. All modern systems are more reliable than the earlier generations of equipment. The contrast and spatial resolution of these systems are in the range of 0.5% and less than 1 mm, respectively. The sophistication of the computer programs that aid in the diagnosis is also remarkable. There are now programs for three-dimensional reconstructions, quantitation of blood flow, determination of organ volume, longitudinal scans (Scoutview, Deltaview, Synerview, and Topogram), and even triangulation programs for performing percutaneous biopsy procedures.

CT units are now being installed in virtually every hospital of more than 200 beds throughout the United States. Most radiologists using these units are generalists who scan all portions of the anatomy. Because of the dissemination of this equipment and its use in general diagnosis, there exists a significant need for a general and complete textbook to cover all aspects of CT scanning. Our book is intended to partially supplement the knowledge of this group of physicians. We have attempted to completely and succinctly cover all portions of CT scanning to provide a complete general reference text. In planning the book, we chose to include the contributions of a large number of talented academicians with expertise different from and more complete than our own in their selected areas. By including contributors from outside our own department, we have been able to produce an in-depth textbook that combines the academic strengths of numerous individuals and departments.

The book is divided into chapters according to the organ systems, except for some special chapters on abscesses and interventional procedures. In each of the chapters the authors have organized the material into broad categories, such as congenital, benign, or neoplastic disease. Each author has tried to cover the major disease processes in each of the general categories in which CT diagnosis is applicable. Specific technical details, including the method of scanning, contrast material, collimation, and slice thickness, are covered in each chapter. The interventional chapter extensively covers the various biopsy and therapeutic procedures in all the organ systems. Finally, the last chapter presents an up-to-the-minute coverage of current and recent developments in the CT literature and also provides extensive information about nuclear magnetic resonance (NMR) imaging. At this time we have had moderate experience with the NMR superconducting magnetic device produced by the Technicare Corporation and have formulated some initial opinions as to its role relative to CT and other imaging modalities. A concise discussion of the physics of NMR and a current clinical status report of the new modality are provided.

We would like to thank all those people who have worked so diligently and faithfully for the preparation of this book. First, we are very grateful to our many contributors. For photography work, we are deeply indebted to Mr. Joseph P. Molter. For secretarial and organizational skills, we are indebted especially to Mrs. Mary Ann Reid and Mrs. Rayna Lipscomb. The editorial skills of Ms. B. Hami were invaluable in preparing the manuscript. Our extremely competent technical staff included Mr. Joseph Agee, Ms. Ginger Haddad, Mrs. E. Martinelle, Mr. Mark Clampett, Mrs. Mary Kralik, and numerous others.

Finally, we are, of course, very appreciative of the support, patience, and encouragement of our wonderful families. In the Haaga family this includes Ellen, Elizabeth, Matthew, and Timothy, who provided the positive motivation and support for this book. Warm gratitude for unswerving support is also due to Rose, Sue, Lisa, Chris, Katie, Mary, and John Alfidi.

John R. Haaga
Ralph J. Alfidi

FOREWORD

I am honored and pleased to write the foreword for the 40th anniversary edition of *CT and MRI of the Whole Body*, a textbook of radiology edited by John Haaga, MD. The esteemed Dr. Haaga has been its editor since its first edition in 1976. Professor Haaga has received a Gold Medal from the American Roentgen Ray Society (ARRS), which is the society's highest honor for distinguished service to radiology. He received this award for his contributions in leadership, teaching, and research, work that he continues to this day. His major innovations include CT-guided interventions that guide biopsies and treatments for abscess, nerve blocks, and cancer. Artifacts from his early work are archived at the Smithsonian Institution. At the age of 36, Dr. Haaga became a tenured professor in the Department of Radiology at Case Western Reserve University School of Medicine and University Hospitals of Cleveland. He later served for 14 years as department chairman at that institution.

He has mentored and taught many hundreds of residents, fellows, and junior faculty members, many of whom have advanced to become distinguished names in their own fields. I am one such beneficiary, having had the fortune of being mentored and guided by John in my early years in radiology. His values and wisdom have allowed me to progress in the field of radiology. I have been inspired to write many books, such as *Genitourinary Radiology: Kidney, Bladder and Urethra, The Pathologic Basis*, published by Springer. I also became Editor-in-Chief of the *Journal of Clinical Imaging Science*, published by Wolters Kluwer.

John is bigger than a film celebrity in India, which I witnessed first-hand when I had the opportunity to accompany him. Everywhere he lectured in India the venue was at capacity. He was literally mobbed by radiology residents wanting to take pictures with him. This book is considered the bible of radiology in India. Every aspiring radiology resident, as well as established faculty, reads this book. I am sure the story is no different in other countries.

CT and MRI of the Whole Body is the largest selling radiology textbook in the world and has been translated into Spanish, Portuguese, and Persian. More than 25,000 copies have been sold in the world. I have been an integral part of this book for the past many years, as I have contributed a complete chapter on *Imaging of the Kidney* and have been Associate Editor for Genito-Urinary Radiology for its fifth edition.

Dr. Haaga, a world renowned radiologist, anchors this book. He has assembled an impressive team of coauthors who are experts in various subspecialties of radiology. The book is divided into four parts: PART I—Principles of Computed Tomography and Magnetic Resonance Imaging, which is further subdivided into sections on Computed Tomography and Magnetic Resonance Imaging; PART II—CT and MR Imaging of the Whole Body, which has seven sections: Neuroradiological Imaging of the Brain and Meninges, Neuroradiological Imaging of the Head and Neck, Neuroradiological Imaging of the Spine, Imaging of the Chest, Imaging of the Abdominal and Pelvic Organs, Imaging of the Cardiovascular System, and Imaging of the Musculoskeletal System; PART III—Image-Guided Procedures; and PART IV—Leading Edge Imaging Concepts.

The sixth edition of Haaga's *CT and MRI of the Whole Body* is a welcome addition. The book is well organized, the chapters are uniformly structured, and each section is richly illustrated. The quality of the paper, printing, illustrations, and figures is excellent. There is ample use of line drawings to explain difficult concepts. The sixth edition of Haaga's *CT and MRI of the Whole Body* is a welcome addition. I am not aware of any other radiology book in the market that is as complete and uniquely illustrated. The cost is reasonable considering the number of illustrations and the quality of work. This book meets the needs of its intended audience. The current edition is completely up to date in the field of diagnostic radiology. It is a must have for radiology residents, radiology faculty, radiology libraries, and serious academic radiologists.

Vikram S. Dogra, MD, FSAR, FESUR, FAIUM, FSRU
Professor of Radiology, Urology & Biomedical Engineering
Associate Chair of Education and Research
Department of Radiology
University of Rochester
Rochester, New York

FOREWORD

Very rarely does a textbook fulfill the promise of being both comprehensive and readable. *CT and MRI of the Whole Body,* edited by Drs. John Haaga and Daniel Boll, not only fulfills that promise, but has continued a legacy of success that has been sustained over multiple editions. It is an honor to have the opportunity to write this foreword. Having trained under the expert eye of Dr. John Haaga, I studied the earliest editions of this book, providing my introduction into the intricacies of cross-sectional imaging. I then had the privilege of watching this true pioneer of CT and MRI take his personal experience and use it to create a resource that has evolved as the field has matured over the past four decades. The current edition of this text covers the wide breadth of CT and MRI anatomically, and the editors have enlisted experts in neuroradiology, head and neck imaging, abdominal imaging, thoracic imaging, musculoskeletal radiology, physics, and a long list of other subspecialties in our field to create a textbook that is as deep as it is broad. With the addition of the energy, talent, and creativity that Dr. Daniel Boll brings to this edition, the result is truly remarkable. I have no doubt that you will agree as you dig into this text, and learn from the combined wisdom of a team of true expert authors, as guided by the steady hands of Drs. Haaga and Boll. Enjoy!

Jonathan S. Lewin, MD, FACR
Executive Vice President for Health Affairs, Emory University
Executive Director, Woodruff Health Sciences Center
President, CEO, and Chairman of the Board, Emory Healthcare
Atlanta, Georgia

Imaging Principles in Computed Tomography

David W. Jordan and John R. Haaga

Computed tomography (CT) has grown quickly from an innovative specialized tool to a mainstay of medicine in every healthcare setting. Hospitals, outpatient clinics, and physician offices find CT to be an essential tool for patient diagnosis and management. Every year brings new advances in CT technology and applications. This chapter is dedicated to the basic principles and physics of CT operation. The practicing radiologist who can evaluate new technology with a good understanding of these principles will be successful in choosing the best tools for his or her practice and in getting the greatest benefit from them.

THE CT IMAGE

Radiography reduces a three-dimensional (3D) body part to a two-dimensional (2D) image with limited contrast, because structures that lie on top of one another are projected onto a single image. The contrast can be improved by using exogenous agents to enhance certain structures or by taking extra projections from different angles to separate the structures in the image plane, but there are limits to how well this can work. The advantage of CT is the improvement in image *contrast* that comes from using a 2D image to show an almost-2D section of the patient without the effect of overlapping structures.

The CT image is a cross-sectional view of the patient rather than an x-ray shadow of the beam passing through the body part (Fig. 1-1). An x-ray beam is used to collect information about the tissues, but the image is not an ordinary projection view from the perspective of the x-ray tube looking toward the film or detector. The image is a cross-sectional map of the x-ray attenuation of different tissues within the patient. The typical CT scan generates a transaxial image oriented in the anatomic plane of the transverse dimension of the anatomy. Reconstruction of the final image can be reformatted to provide sagittal or coronal images; these are viewed from the same perspective as a digital radiograph, but they show thin slices of tissue rather than superimposed tissues and structures. The pixel values show how strongly the tissue attenuates the scanner's x-ray beam compared to the attenuation of the same x-ray beam by water.

The CT image is produced by the process of *reconstruction:* digitally combining information from x-ray projections through the patient from many different angles to produce the cross-sectional image. Because the image is digital, it is made up of a group of *pixels* (shortened from "picture elements"). Each pixel has a grayscale value that is displayed to the viewer. The image is 2D, but it represents a 3D volume of tissue with a finite thickness (usually a very small thickness compared to the field-of-view (FOV) size [≈2-5 mm]). Each pixel is the projection, or 2D representation, of the x-ray attenuation of a *voxel* (shortened from "volume element") of physical tissue. The size of the pixels and the thickness of the voxels relate to some important image quality features, such as detail, noise, contrast, accuracy of the attenuation measurement (CT number value), and artifacts. These will be discussed in more detail as they relate to the processes of acquiring and reconstructing CT data.

CT ACQUISITION OVERVIEW

The basic process of collecting data in CT is illustrated in Figure 1-2. In a CT of a single section of tissue using a single detector, the x-ray beam is collimated to the desired image thickness. The detector array has a number of individual detector elements that each record the intensity of the beam passing through the tissue along the path from the x-ray tube to the element. The system captures a simple projection x-ray through the patient, consisting of a thin strip or row of pixels. It can be thought of as a one-dimensional (1D) radiograph. The scanner then rotates the source and detector to capture additional 1D "strip x-rays" through the same section of the patient, viewed from a number of angles. Each strip radiograph *(projection)* is stored in the computer memory for later reconstruction.

In *multislice CT* (Fig. 1-3) this operation is performed simultaneously for many arrays of detectors stacked side by side along the z-axis (long axis) of the patient. The x-ray beam collimators can be opened so that a wider section of the patient is irradiated, and each row of detectors can measure a separate transmission signal for the tissue section that lies between the detector row and the tube. The width of tissue that is sampled by each detector row is determined by the physical width of the detector elements along the z-axis.

CT images and individual rotations of the scanner gantry are often called *slices* because a single data acquisition and reconstruction produces an x-ray map of a thin section of the patient's body. The tissue displayed in the image represents the same tissue as if a thin slice or section of the patient's body were cut in a plane perpendicular to the long axis (superior-inferior) of the patient's body and fixed for viewing. Early CT scanners collimated the width of the x-ray beam to the width of a slice (e.g., 5 mm), irradiated one slice at a time, and collected data for transmission through one slice at a time. Multislice scanners use a wider beam to cover more tissue with each pass of the tube, and the detectors contain arrays that are arranged to collect data for multiple individual adjacent slices at the same time. The detector element(s) for each slice store data separately and represent different physical sections of tissue.

The term *slice* can be confusing because in common use it can refer to several different things. When a CT scanner is called a "16-slice" model, it usually means that the scanner can acquire up to 16 individual detector data sets at one time. It is more precise to call this a *16–detector row* CT scanner. The individual data elements acquired should be referred to as *acquired images* or *acquired projection data.* In a multidetector-row scanner, the data are often acquired in thicknesses of 0.5 to 0.7 mm and reconstructed in image thicknesses of 3 to 5 mm.

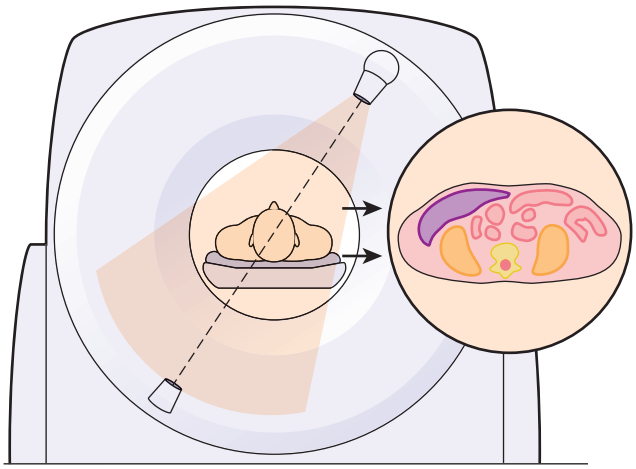

FIG 1-1 A CT image represents a cross section of the imaged subject rather than the x-ray shadow of the anatomy, as in a conventional radiograph.

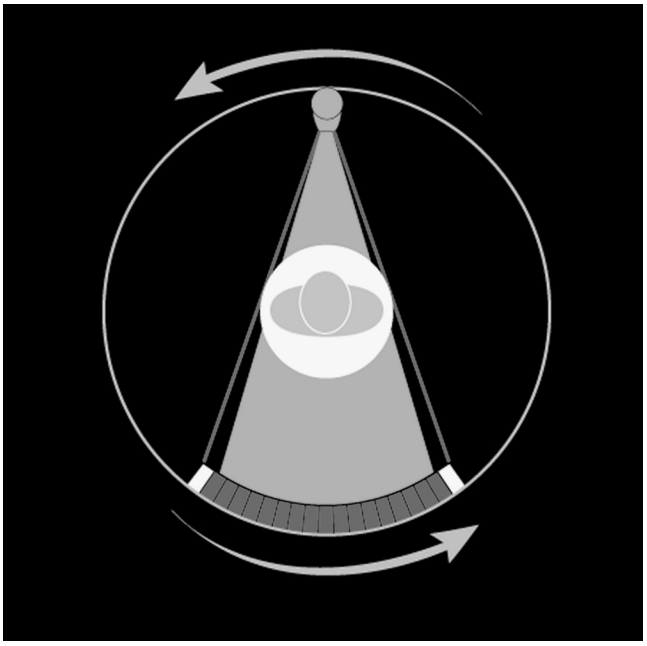

FIG 1-2 A simple CT scan produces a one-dimensional strip radiograph for each projection through the patient.

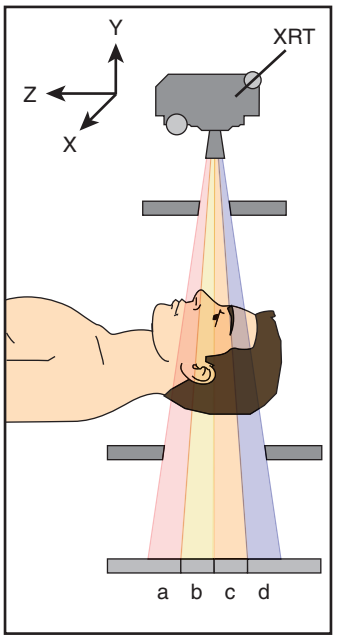

FIG 1-3 In multislice CT, several independent detectors arranged side by side sample data from unique locations within the x-ray beam.

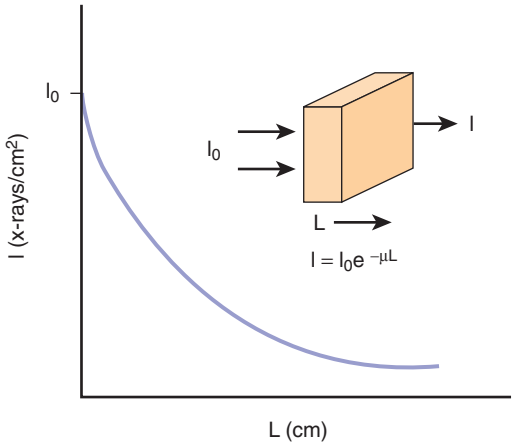

FIG 1-4 Exponential attenuation of x-ray beam intensity in an absorber, such as tissue.

The images that are presented to the operator or physician for viewing should be called *reconstructed images,* although many people continue to refer to these as *slices.*

Linear Attenuation and Projections

The fundamental x-ray physics of CT are the same as those for radiography. A source of ionizing radiation is transmitted through an object to recreate an image of the object based on its x-ray absorption (Fig. 1-4). The intensity of the transmitted radiation beam is given by the equation:

$$I = I_0 e^{-\mu x}$$

where:

I_0 is the incident intensity of an x-ray beam on the surface of an object of thickness x

I is the transmitted intensity

e is Euler's constant (2.718)

μ is the linear attenuation coefficient

Attenuation of an x-ray beam with a particular spectrum depends on two distinct properties of the tissue: the atomic number and the density of the attenuating material. When collecting one projection, it is not possible to determine what combination of atomic number and density resulted in the measured attenuation. Thus both very dense materials (e.g., bone) and materials with a high atomic number (e.g., iodine contrast media) produce strong attenuation. Both would have a similar appearance on CT even though they have very different physical properties. The key advantage of dual-energy and spectral CT techniques (discussed later) is that they can be used to probe the attenuation arising from density and atomic number separately by making two different measurements of the same sample, object, or body part.

The transmission of the beam (the ratio $I:I_0$) determines the signal that is collected by the CT scanner detectors at each projection angle, and the attenuation differences along different paths through the patient's body result in the patterns that are formed in the data for each projection acquisition.

CT Reconstruction and Image Display Overview

Once the 1D projection radiographs have been collected, they are transformed into the cross-sectional image to be displayed to the user. There are several approaches to image reconstruction, broadly classified as *filtered backprojection* (FBP) and *iterative reconstruction* (IR) techniques. All of these methods use computerized mathematical operations to combine the 1D projection attenuation information into 2D maps of the attenuation of the scanned subject.

CT Number Scale

The reconstructed CT image is a map of tissue attenuation, and these maps are quantitative owing to the use of a scale called the *Hounsfield unit* (HU) scale. The scale is named for the inventor of the x-ray CT scanner, Sir Godfrey Hounsfield. The HU scale is a relative scale for linear attenuation of the tissues. It is valuable to quantify the pixel values so that the physician can compare the composition of one tissue with another.

The HU scale is based on relating all measured attenuation values to the attenuation of water. A CT numbering system that relates a CT number to the linear attenuation coefficients of x-rays in different absorbers compared to water is given by:

$$\text{CT Number} = \frac{K(\mu - \mu_w)}{\mu_w}$$

where:

μ_w equals the attenuation coefficient of water

μ is the attenuation coefficient of the pixel in question

When K = 1000, the CT number scale is the HU scale. Other K values can be used to change the scaling of the entire system. When the HU scale is used, air has a value of −1000 HU, water has a value of 0 HU, and dense bone has a value of +1000 HU.

The advantage of the HU scale is that density differences of 1 part in 1000 (0.1%) can be represented by distinct values. The inherent density resolution of CT scanners is about 0.5%, so the HU scale is sufficient to display all attenuation differences the scanner can measure. Increasing the value of K would not improve on the density resolution of the system.

As a general rule, the human eye cannot appreciate contrast differences of less than about 10%, whereas CT scanners can easily demonstrate differences of less than 1%. Thus the small density-resolution difference measured by the CT scanner must be exaggerated for viewing. This is accomplished by enabling the user to select a small range of gray levels from the entire CT number scale and to reset the black and white limits. This is done automatically for many scanners by presetting an appropriate "window/level" setting to be used for display; this setting can be modified by the user, both on the scanner and when the image is displayed on other workstations and picture archiving and communication systems (PACS).

GENERATION OF A CT IMAGE

Components of a Data Acquisition System

Gantry. Modern CT systems use slip ring technology to permit the scan frame to rotate continuously for spiral or helical CT scanning. Slip rings are used to transmit power and some control signals to the system components mounted on the gantry rotor. Systems with many detector elements and data input channels use broadband wireless communication to transmit collected image data from the detector assembly to a receiver on the stationary base of the scanner.

To enable high-speed scanning with good temporal resolution, CT system developers have focused on providing high gantry rotation speeds. For high-performance systems with mechanical roller gantry bearings, gantry rotation times of 0.33 seconds are achievable.[63] Operating modes are available to acquire data over a partial arc (<360 degrees) to shorten the apparent rotation time further. Air bearing technology[52] enables even faster rotation speeds. Scanners with air bearing gantry designs can achieve rotation times of 0.27 seconds.[20] Such rotation speeds are desirable to achieve cardiac imaging without using β-blockers to slow patients' heart rates. Together with large-coverage detector arrays, subsecond scan times permit rapid acquisition of contiguous anatomic areas for volume data acquisitions.

X-Ray Generators and Tubes. High-frequency x-ray generators are required to produce intense x-ray beams for high-speed scanning. Typical operating frequencies range from 20 to 50 kilohertz (kHz).[32] Generator power ratings of 80 to 120 kilowatts (kW) are common, as shown in the manufacturer specification charts for commercial systems available in the United States. Most generators support a wide range of exposure techniques from 80 to 140 kilovolts (kV) and 30 to 500 milliamperes (mA). Some generators have a lower tube potential option (70 kVp) available as an approach to radiation dose reduction. Generators are located on the rotating scan frame within the CT gantry, together with the x-ray tube and detector assembly, and are powered by a low-voltage power supply provided via the slip ring.

Modern generators have a number of features to enable them to adjust and optimize radiation output and image characteristics in real time while scanning. The generator design is computerized and flexible to allow for computer-controlled x-ray techniques generated by the scanner's master control computer. Modulation of tube current based on patient thickness is a standard feature. Scanners may have the ability to vary the tube current along the z-axis of the patient, in the x-y plane, or both. Some systems allow dynamic or automated selection of kVp based on patient size and/or study type.[10,37,49,62] For dual-energy (spectral) imaging, one approach that relies on a high-performance generator is fast kV switching.[29] The generators for these systems can toggle rapidly (≈150 msec) between two operating voltages (usually 80 kVp and 140 kVp).

Modern CT scanner x-ray tubes have rotating anodes and use innovative cooling methods to continuous high x-ray output. Many tubes feature focal spot modulation or "flying focal spot" technology.[14,15,35,57] These tubes, in addition to providing large and small focal spots, have the ability to rapidly shift the position of the selected focal spot during the scan. This has the effect of changing the sampling behavior of the scanner to enhance the resolution of the image data. Tube ratings for typical modern CT scanners can have 30 million heat units (30 MHU) of heat storage capability and a continuous output power capability of 120 kW.

Filters. CT scanners have x-ray filters to shape both the geometry and spectrum of the beam. The standard filter is made of aluminum, like a radiographic tube filter, but there are important differences in the filter design. CT filters are generally thicker than radiographic filters and often combine other materials (e.g., Teflon, copper) with aluminum. The CT beam is much "harder" than a radiographic beam at the same kVp—it contains fewer low-energy photons and the average energy is much higher (Fig. 1-5). This is done to reduce patient radiation dose (because low-energy photons are more likely to deliver dose to the patient without contributing to the image). In radiography the

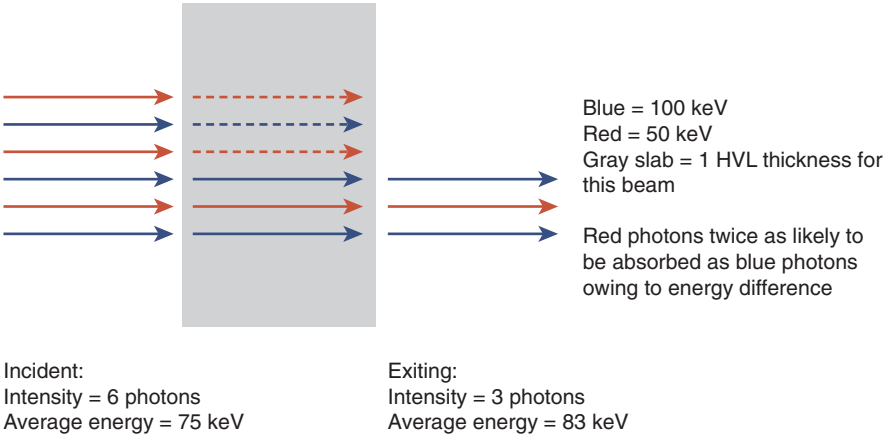

FIG 1-5 Beam-hardening example. A beam composed of different photon energies passing through one half-value layer of absorber will have a lower intensity (fewer photons) and a higher average energy in the transmitted beam, because the low-energy photons are more easily absorbed and the high-energy photons are better able to penetrate the absorber.

lower-energy photons help provide contrast to the image, but CT has much higher inherent contrast sensitivity than radiography, so a useful image can be obtained without the lower-energy photons.

The compensating filters used in CT are often called *bowtie filters*[59] because of their shape. The filter is thinnest at the central ray of the beam and thicker toward the azimuthal edges of the fan beam. Thus the thinnest part of the filter is in line with the thickest path length through the patient's body as the gantry rotates, and the thicker part of the filter is in line with the thinner peripheral anatomy (peripheral). The filter partially compensates for the patient's body thickness contour. The result is that for any line across the FOV, the total attenuation and beam hardening along the x-ray path is much more uniform than if the beam only passed through the patient. Compensating for the attenuation differences allows the scanner to operate with a smaller dynamic range at the detectors, and compensating for the beam hardening improves the scanner's quantitative accuracy in representing tissue attenuation as CT number values (HUs). A scanner will have at least two different bowtie filters to provide compensation for head and body scans, and some scanners have as many as five or six different filters to match a variety of patient body sizes. The bowtie filter is selected by the scanner and switched into the beam path automatically based on the scan setup chosen by the operator.

Detectors. CT scanners use scintillation crystals to convert x-rays to visible light pulses, which in turn can be detected and counted by electronic circuits. Conventional detectors produce light pulses and voltage pulses, resulting in a simple count of x-ray photons detected. Research is underway to develop photon counting devices that can detect the number of x-ray photons as well as information about the energy of each individual photon.

CT detectors use crystals composed of fast scintillator ceramics such as cadmium telluride[28] and gadolinium oxysulfide.[64] Development of new crystal materials is an active area of research to further improve scanner performance, and each CT manufacturer has newer proprietary crystal types available or in development. The crystals convert x-rays to light pulses whose intensity is proportional to the total energy of photons striking the crystal. The light is converted to current and hence a voltage across a resistance, which in turn is detected as digital data for use by the reconstruction system. This multistep process of analog signal conversion to digital data produces a number of errors and inefficiencies related to quantization error, sampling and recovery speed, and electronic noise.[21] Despite these inefficiencies, even primitive CT devices can measure low-level signals accurately over a wide dynamic range with great precision, permitting reliable imaging of diverse density extremes such as bone, air, and water.

Detector arrays continue to grow as individual detector elements remain small, providing small pixel size with ever-greater anatomic coverage. Common detector arrays accommodate scanning of 80 to 160 mm of coverage in a single tube rotation, with resolution of 0.5 to 0.6 mm, so that entire sections of patient anatomy can be captured in a single revolution of the CT scanner's rotating frame, taking less than 1 second.

Because of the fixed position of the tube/detector combination, the associated detectors and electronics system must be stable, uniform, and capable of tracking over a wide dynamic range. Noncompensation for errors as small as a few thousandths of 1% can cause visible (ring) artifacts.[34] In addition, spatial resolution, a key image quality parameter of CT (see later), can be limited by the data sampling. In this geometric relationship, the number of detectors in the arc or array determines data sampling; that is, spatial resolution depends on how closely spaced the rays are in each view.

The typical number of detectors in the array ranges from about 600 to more than 900. These numbers result in limiting spatial resolution of approximately 5 to 10 line pairs per centimeter (lp/cm), depending on the reconstruction type (filter), reconstruction matrix size, and scan FOV. Sampling theory requires that to visualize a particular object, the sampling frequency must be at least twice the spatial frequency associated with the object.[26] In practice even higher sampling rates are desirable. Axial resolution of greater than 5 to 10 lp/cm (0.5-1.0 mm) may be limiting for specific clinical applications.

Data Acquisition Systems

Data acquisition systems (DAS) are the heart of CT scanners. These systems perform detector signal analog-to-digital conversion and data preprocessing for the scanner's reconstruction system. Steps performed by the DAS include conversion of electric current (from the detector) to voltage, digitization of voltage pulses, subtraction of background offset signal, logarithmic conversion of data, and transmission of data to the preprocessing system. In modern systems, these functions are

integrated and combine multiple steps on specialized hardware—boards, chips, or modules integrated into detector modules that can be housed on the detector assembly within the rotating scan frame.

An ideal DAS would accurately and consistently digitize the input signal from the detectors with no noise. The inherent electronic noise produced within the DAS must be small enough that the total noise in the sampled signal depends mostly on the x-ray quantum noise. The DAS must also have a wide dynamic range and be as linear as possible across the range of possible input signals so that the x-ray beam intensity can be accurately determined for the range of available x-ray outputs as well as a wide variety of attenuation types (tissues) and thicknesses.

A DAS will have some dark current that can vary with temperature and over time, affecting the precision (reproducibility) of the detector signal measurement. A low dark current that is stable with ambient temperature changes is desirable. Crosstalk limits the DAS performance when residual signal from one sample is collected as part of the next sample. A high-performance DAS must be capable of high sampling rates with low crosstalk.[21]

Scanner Operation and Data Acquisition

Rotate/Rotate Scanner Geometry. During the development of CT, several combinations of x-ray tube and detector movement were used to collect data. The historical significance of each is described in previous editions of this book. The rotate/rotate geometry emerged as the best practical design choice for high-speed scanning in multidetector-row systems and is the geometry used currently in modern multidetector CT systems.

In a rotate/rotate system the x-ray tube and detector array are mounted opposite each other on the rotating scan frame as shown in Figure 1-2. A wide-angle fan-beam geometry (50-55 degrees) is used, and an arc of detectors and the x-ray tube rotate continuously around the patient for 360 degrees. Projection data (or data samples) are obtained at various angles, and for each angular sample taken at a position of the tube and detector, a view is created.

In rotate/rotate geometry, the detectors are fixed radially and do not view the scan area uniformly. Only the center detectors in the array "see" the pixels at the center of the FOV. However, this fixed relationship allows the detectors to be highly collimated, which greatly reduces detection of scattered radiation; this maintains contrast in the image so that the viewer will be able to detect objects against a higher background of image noise (or mottle, or grainy background).

To overcome the limitations of detector size on spatial resolution, manufacturers have developed various methods that exploit the scanner geometry. One method of increasing spatial sampling (and spatial resolution) is to offset the detector array relative to the center of rotation by a quarter-ray or eighth-ray. This allows data collected during the second half of a 360-degree rotation to be interleaved with that of the first half, effectively doubling the sampling and resolution. Patient motion can reduce this benefit. In addition, this method is limited in spiral CT scanning to certain modes in which data from projections acquired through 360 degrees are available for interleaving.

Another effective method of increasing data sampling is to oscillate the x-ray tube focal spot a few millimeters during a scan (Fig. 1-6) to achieve interleaved data samples. The position of the focal spot is accurately controlled and synchronized with rotational speed and position of the rotating frame. Data acquired during the use of each focal spot position are stored separately and then interleaved to provide greater spatial sampling of the tissue. This approach can be used to increase sampling within the scan plane as shown in Figure 1-6, and can also be used to provide increased sampling along the z-axis.[14,35] When focal spot modulation is done along the z-axis, the finer sampling can be used to produce sagittal and coronal reformatted images with smaller pixel sizes than would be possible with the physical detector elements alone. Systems with this capability are often marketed as having more "slices" than the number of actual detector rows available on the scanner; for example, a scanner with 32 detector rows may be marketed as "64 slice" or a scanner with 128 detector rows may be marketed as "256 slice."

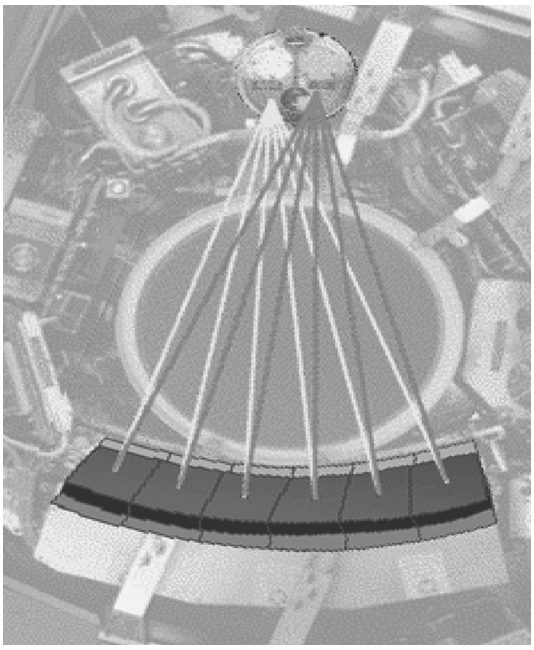

FIG 1-6 The dynamic or "flying" focal spot technique is used to provide finer effective spatial sampling of tissue.

Spatial resolution requires adequate view sampling to prevent aliasing artifacts. Views (angular projections) are limited by the electronic measurement capability of the scanner, which is typically not the gating factor for maximum resolution. These factors vary for every CT manufacturer and can dramatically affect the overall performance of a scanner.

Spiral (Helical) Scanning. Until the late 1980s, CT scanners acquired data in discrete slices of patient anatomy in a method commonly called *axial scanning*. In axial (cross-sectional) CT, each revolution of the x-ray tube around the patient produces a single data set (slice). During data collection, the patient table is motionless. To create an additional slice, the table is translated by a given amount and the x-ray tube rotates around the patient again. Each rotation produces a single image. The advent of slip-ring technology and new data reconstruction techniques enabled spiral, or helical, CT.

In spiral/helical CT, the patient table translates through the gantry while the scan frame rotates continuously around the patient, sampling data as a volume. This permits new options in reconstruction. For example, once a volume of data is collected, an image can be reconstructed at any point along the effective path traced by the x-ray tube. There are several key terms associated with helical scanning:

Acquisition is the entire volume of data collected during a continuous spiral scan.

Revolutions refer to the number of 360-degree rotations of the x-ray tube during a single acquisition.

Pitch is the distance the couch travels during one 360-degree revolution of the x-ray tube divided by a length associated with the x-ray beam and/or data acquisition. The most common value

used (as in the International Electrotechnical Commission [IEC] definition) is the width of the collimated fan beam along the z-axis of the scanner.

Interpolation is a reconstruction method (most accurately described as "deconvolution") that permits the realignment of spiral/helical scan data for reconstruction of an axial (cross-sectional) slice.

Spiral CT has many advantages over conventional or axial CT, including:

- The ability to minimize motion artifacts owing to faster/shorter acquisitions
- Decreased incidence of misregistration between consecutive axial slices
- Reduced patient dose
- Improved spatial resolution in the z-axis
- Enhanced multiplanar or 3D renderings

Motion artifacts are minimized in spiral CT because of the faster scan times associated with the examination (versus step-and-shoot axial scanning); many spiral CT examinations can be completed in a single patient breath hold. The faster scan times associated with spiral CT also permit accurate slice-to-slice registration and eliminate the misregistration associated with inconsistent breath holds in conventional axial scanning. Reconstructions can be overlapped or ideally positioned for accurate visualization of small lesions.

Spiral scanners achieve reduced patient dose by extending the pitch factor for a given study. For example, consider a typical thorax, abdomen, or pelvis examination. Typical slice widths range from 2 to 5 mm. With spiral CT, the same examination with the same slice thickness as axial CT can be completed with 50% greater table speed using a pitch of 1.5; this results in a 33% reduction in patient dose (Fig. 1-7). The downside to this approach is a slight broadening of the slice sensitivity profile (effective axial slice thickness) based on the type of spiral reconstruction chosen. This limits the spatial resolution along the z-axis, which can reduce the detail available in sagittal or coronal reformatted images.

With continuous collection of data, spiral CT enables a reduction in image-to-image separation, thus improving spatial resolution in the z-axis if the data are oversampled (pitch < 1.0). Although axial CT might overcome this challenge by overlapping consecutive axial acquisitions, this would lengthen scan time needed to cover a given region of patient anatomy more than doing so in a helical acquisition.

Spiral CT data acquisition systems must be capable of collecting large volumes of data at extremely fast data rates. Data sampling for most systems is in the range of 3 kHz and can provide up to nearly 2400 projections or views per rotation of the gantry. Data rates for many new systems exceed 200 megabits/second. This extremely fast sampling capability enables high spatial resolution and enhanced z-axis sampling of patient anatomy.

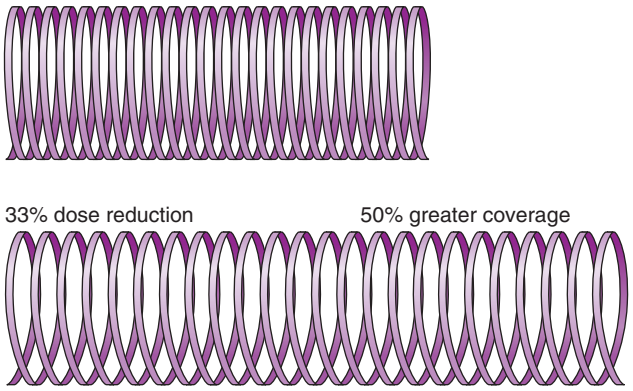

FIG 1-7 Increasing pitch decreases radiation dose and increases the scan coverage that can be achieved in a given scan time, using the same rotation speed and number of rotations.

The increased speed of data acquisition systems and a number of other technologic developments paved the way for data acquisition at subsecond rotation speeds of the rotating frame. Subsecond spiral data acquisition permits temporal resolution on the order of 220 to 300 milliseconds, depending on the scanner manufacturer. These temporal resolutions enable more examinations to be scanned within a single breath hold and increase the range of anatomy that can be covered in a single acquisition. This improves the performance of clinical applications such as CT angiography, which requires precise timing of a contrast bolus injection and rapid acquisition during the arterial phase. Fast data acquisition can also improve the z-axis resolution for a given study by covering the same amount of anatomy in the same time with thinner slices and/or with oversampling at low pitch.

Multidetector-Row Designs. Multidetector-row scanners are motivated by the desire to cover large regions of anatomy in short times with fine sampling along the z-axis of the patient. In early scanners with only a single data acquisition channel (single slice), the beam width directly determined the coverage as well as the image thickness (spatial resolution). With the development of fast, stable, compact electronics, it became possible to build a DAS that could simultaneously acquire and store multiple images. By arranging multiple narrow detector rows side by side along the z-axis, connecting them to a DAS with multiple input channels, and increasing the x-ray collimation width to cover the entire assembly, scanner designers provided users with more flexibility to achieve faster scans or finer spatial detail.

The first deployment of this technology included a dual-arc detector as shown in Figure 1-8. In this configuration, two parallel arcs of detectors are used to acquire data simultaneously during a single revolution of the scan frame, dividing the total x-ray beam into two equal beams defined by the detector aperture of each row of detectors. Considering small gaps between rows, which can be ignored from the perspective of data acquisition, the total x-ray beam collimation now becomes the sum of detector row collimations (Fig. 1-9). This concept can be extended to for systems with multiple rows of detectors.

Early multidetector-row systems were commonly equipped with a four-channel DAS. Such systems were often referred to as "four-slice" CT scanners because they could collect up to four images simultaneously in a single rotation of the scan frame. A user upgrading to such a system from a single-detector system would have the flexibility when imaging 5-mm slices to increase acquisition speed or to use finer spatial sampling in the z direction. Configuring the scanner to simultaneously acquire four 5-mm images in each rotation using a 20-mm beam collimation would reduce the acquisition time by a factor of 4. Alternatively, sampling the data using four 1.25-mm detectors and reconstructing 5-mm images would accomplish the scan in the same period of time, but the data available for sagittal and coronal reconstructions would have finer sampling and thus a smaller pixel dimension in the z direction. A possible scheme of detector configurations for such a four-channel system is shown in Figure 1-10.

This tradeoff between coverage and z-sampling affects systems with 2 to 16 detector rows, and such systems were designed with different available combinations of physical detector element sizes, DAS input configurations, and x-ray beam collimation widths to provide clinically useful choices. Two detector designs have been deployed by CT manufacturers, unequal width and equal width, referring to the sizes of the individual detector-row elements across the z dimension of the

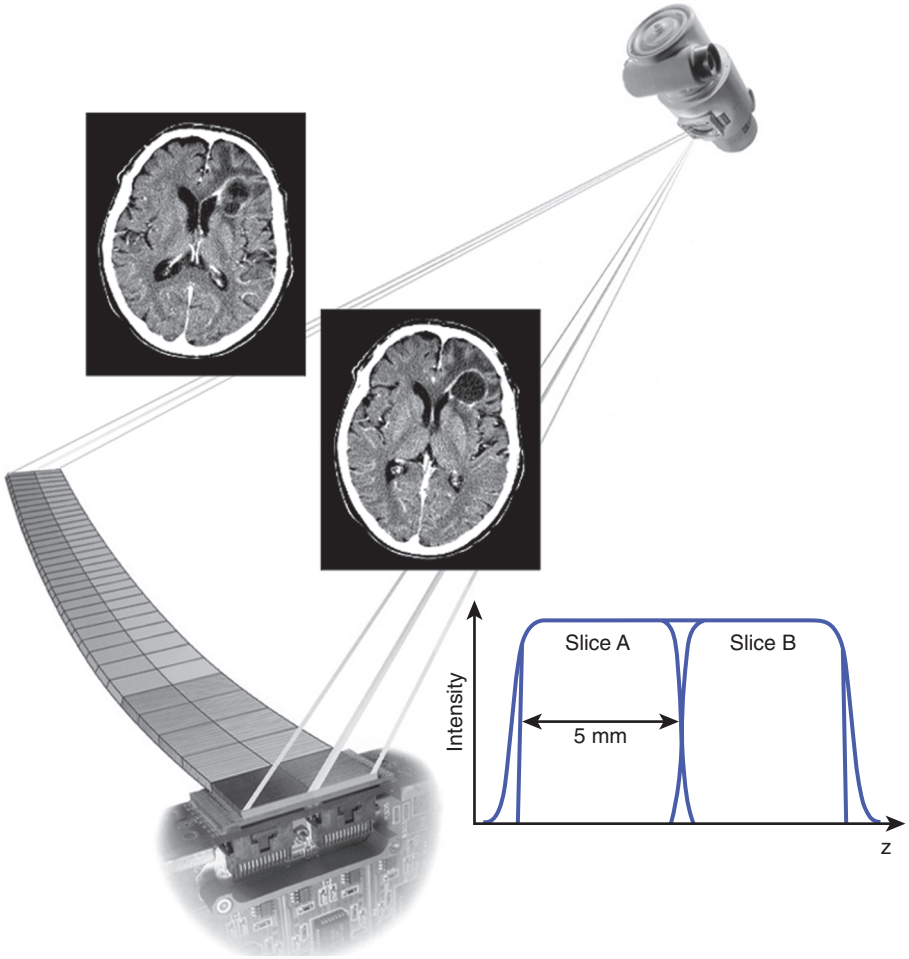

FIG 1-8 Early multislice detector system with dual-row detector. (Courtesy J. S. Arenson.)

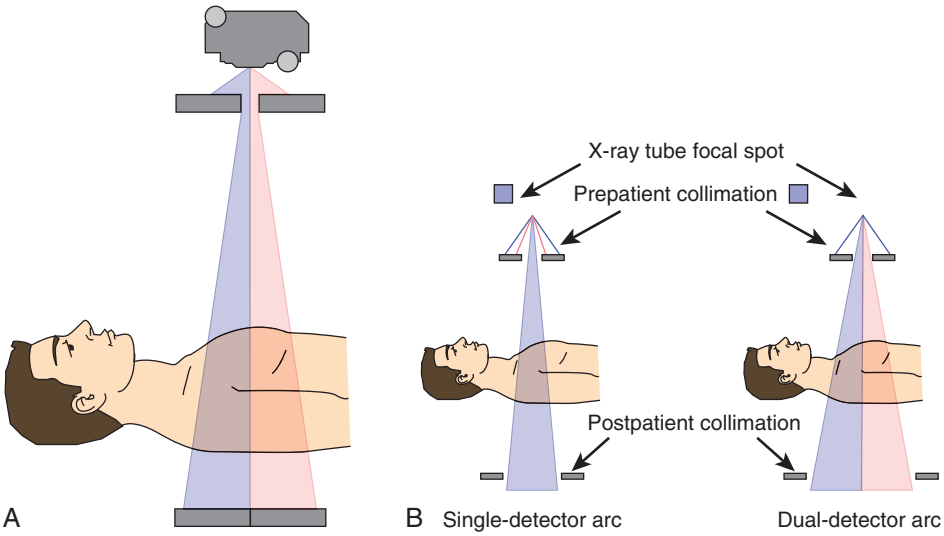

FIG 1-9 **A,** Arrangement of a dual-row detector array along the z-axis of the patient. **B,** Total x-ray beam width (source collimation) is the sum of the consecutive detector row widths along the z-axis.

detector array. In systems with unequal-width detector designs, the center of the detector array contains smaller detector elements that can be connected individually to the DAS for fine z-sampling with individual detector channel widths such as 0.5 mm, 0.625 mm, or 1.25 mm. The outer elements are larger and are used for wide coverage applications; in such configurations, several small center elements are electronically combined into one DAS channel. For example, one DAS channel could connect to a single outer-row element with 2.5-mm width, while another DAS channel could collect data from four 0.625 elements acting as a single 2.5-mm element. In this arrangement, the

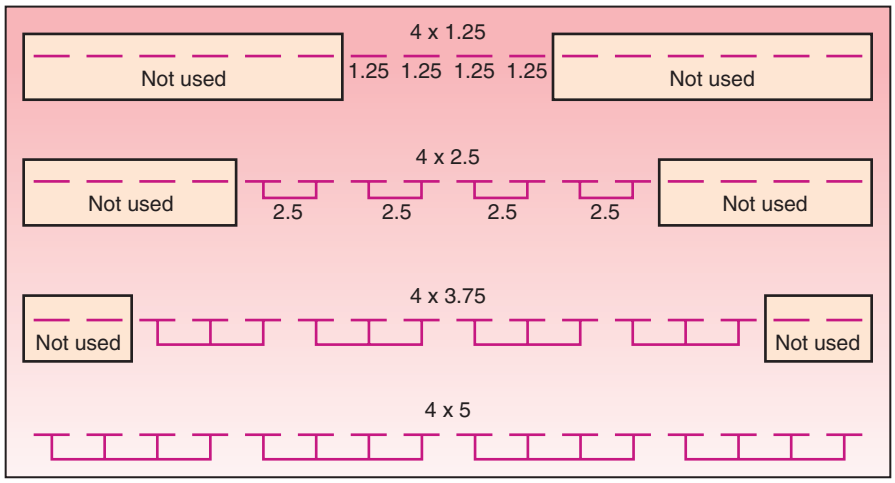

FIG 1-10 Matrix detector with 4-channel DAS. Electronic combination of individual 1.25-mm elements produces slice width configurations of 4 × 1.25 mm, 4 × 2.5 mm, 4 × 3.75 mm, or 4 × 5 mm.

data from the four 0.625-mm elements cannot be recovered as individual z-samples, because they are combined at the input to the DAS, so the effective z-sampling is based on 2.5-mm channel widths for this scan. An alternative design is the equal-width design, where all of the detector elements have the same physical width and are connected to individual DAS channels or grouped in combination depending on the application and the needed resolution and coverage. For systems with more than 16 detector channels, it is possible for most applications to use an equal-width detector with submillimeter elements (0.5 mm or 0.625 mm are common) and provide isotropic z-sampling across the entire detector array with wide coverage. For example, a 64-detector-row system with 0.625 mm detectors can sample 40 mm of coverage with each scanner rotation while providing a separate DAS channel for each individual detector row.

Multirow detector arrays have rapidly progressed from having 2 or 4 detector rows to 64, 128, 256, and up to 320 rows in commercial CT systems. This is possible because the miniaturization of electronics enables more detector and DAS components to be installed in a detector assembly that can be practically attached to the rotating scan frame, given its size and weight. Systems with many detector rows also require advanced low-power-consumption electronics or larger power supplies to support the detector and DAS; practical limitations on these systems include providing adequate cooling for the electronics within the scanner housing. These systems use a wireless link to transfer data from the DAS on the rotating frame to the scanner's reconstruction system, so capturing many channels of data simultaneously with high sampling rates requires a high-throughput wireless link. Advances in high-speed wireless data technology have enabled the 256- to 320-channel configurations in use in current systems, and it is possible that still larger numbers of data channels will be used the future.

CT TECHNIQUE FACTORS

CT technique factors are the settings that are selected by the operator at the scanner's control panel. Each has a specific effect on radiation dose to the patient and the characteristics of the scanned images. The technique factors for a scan describe the x-ray beam parameters and the geometry of the scan.

The x-ray technique factors in CT are familiar from conventional radiography. The kilovoltage (kV) applied to the x-ray tube and the tube current (mA) are selected by the operator. The exposure time is usually chosen to be the time of one complete 360-degree rotation of the rotating scan frame, so the speed of the rotation is adjusted for each scan to achieve the desired exposure time. These typically range from 0.4 to 1.0 seconds, although shorter times and faster speeds are possible.

The selection of a helical (spiral) or axial (step-and-shoot) scanning mode is a key technique factor for the scanning geometry.

The collimation of the x-ray beam along the z-axis is normally not selected directly by the operator, but rather is chosen by the scanner to match the detector configuration. *Detector configuration* refers to the size (length along the z-axis) of individual data acquisition channels and the total number of such channels or rows along the z-axis. For example, 64 rows of 0.625-mm detectors (N = 64, T = 0.625 mm) would be used with a total collimated beam width of 40 mm. On some systems the user may select the detailed detector configuration to achieve a certain degree of z-sampling/spatial resolution for multiplanar reconstructions. The scanner software will often choose a detector configuration automatically based on the selected reconstructed image thickness.

The pitch is a geometric technique factor in helical scanning. The coverage and scanning speed can be determined from N × T, rotation time, and pitch (for a helical scan). In this way, faster rotation speeds and wider beams covering greater z extent of the patient are used to achieve faster scans of a given anatomic region.

The scan FOV is chosen to approximately match the body size being scanned. On some scanners there are only two modes (Head and Body); other scanners have an array of SFOV size choices to contour to various patient sizes and body parts more closely.

Automatic exposure control and tube current modulation are particularly critical for radiation dose management in modern CT. These technologies usually have a few parameters and settings to control how they operate. Use of these tools and the settings used make up part of the technique factors.

Although not technically part of technique factors, reconstruction, postprocessing, and display techniques all have a dramatic impact on the quality and appearance of the images that are eventually produced.

Automatic Tube Current Selection and Modulation

In an ideal scenario, dose and image quality would be optimized by delivering the same x-ray beam flux to the detector for every projection

through the patient. Of course the density and width of a patient's body can vary greatly within a region of interest, especially when scanning an entire body region (or multiple regions). Using a single fixed mAs value does not achieve the needed optimization; some anatomy will necessarily be depicted with inadequate image quality or exposed to excess radiation in this approach.

Automated tube current modulation (ATCM)[30] is a tool to address this challenge. Ideally ATCM can be used to optimize the scanning parameters in real time so that each patient is exposed to just enough radiation to produce a diagnostic-quality image—and no more. Automating this process should remove variation among users and the possibility of user error. The technology can be subdivided into three related techniques: automatic tube current selection, varying the tube current along the z-axis of the patient, and varying the tube current in the x-y plane around the patient.

Automatic tube current selection[1,31,36,40,47,56] (ATCS) is usually done by analyzing the scout/topogram image or images to estimate the attenuation of the patient and select an appropriate mAs value. The specific implementation on any given scanner may require a posteroanterior/anteroposterior (PA/AP) scout image, a lateral scout image, or both. Given the differences in patient dimension and density along a frontal versus a lateral projection, using both images should produce the most accurate choice of the correct mAs. In real implementations, most single-scout tube current modulation schemes are accurate enough.

The attenuation of the patient as measured from the scout image can be measured and expressed as the water-equivalent diameter (WED) of the patient.[39] The WED is the diameter of a water-filled cylinder that would produce the same x-ray attenuation as the patient cross-section. This value can be very different from the physical dimension of the patient, especially in regions containing large areas of low attenuation (chest) or high attenuation (pelvis). Once the patient's WED is determined by the scanner, the scanner chooses an mAs value based on the image quality parameter chosen by the user. In some cases this is done by specifying a target image noise value; the scanner uses calculation or lookup tables to determine what mAs value will produce the target noise for the chosen kVp and the estimated patient WED. In other cases, this is done by specifying a target or reference mAs value. In the reference mAs implementation, the reference mAs value actually represents the amount of image noise produced when a reference WED (e.g., 24 cm) is scanned with the specified mAs. Thus when a user specifies a reference mAs value of 200, what they are actually doing is asking the scanner to use an mAs value to scan the patient that will produce the same amount of noise that 200 mAs produces in the reference WED.

When using ATCS it is important to understand the specific functions as implemented by the scanner manufacturer. There are differences among commercial implementations in how the scout images are used to determine the estimated patient WED. Some scanners use the PA scout, some use the lateral, some use both, some use the first scout acquired during the examination, and some default to a fixed mAs if the expected projection (i.e., PA) is not performed first. This can lead to important workflow considerations for the technologist performing the scan. It is also important to know when designing and setting up scan protocols and technique factors on the scanner.

Z-axis tube current modulation (zTCM) is closely related to ATCS and is used to vary the tube current during each rotation of the tube, based on the different attenuation properties of different body regions. This is usually done using the estimated WED determined from the scout image. Once the baseline tube current has been established, either using automated selection or manually, zTCM is used to increase or decrease the tube current during tube rotations covering portions of the body with higher or lower attenuation. The simplest example is a scan of the chest, abdomen, and pelvis. The manually or automatically selected baseline tube current would likely be the value used to scan the abdomen, whereas a reduced current would be used in the less-dense chest and a higher current would be used to achieve good beam penetration through the dense bones in the pelvis region.

X-Y, or azimuthal, tube current modulation (aTCM) allows a further degree of fine-tuning of the radiation output to match the projection attenuation. Once the tube current is chosen to achieve a target noise level and varied based on the general density of the body region, there is still a large difference in attenuation between lateral projections and AP/PA projections. This difference is pronounced for most of the chest, abdomen, and pelvis when patients are imaged in supine or prone positions, and is especially pronounced in the shoulders and hips because of the dense bones that are superimposed in lateral projections. For scanners capable of varying the current within a single tube rotation, a modulation scheme may be available to reduce the current for AP and PA projections and increase it for lateral projections. In a variation of this approach, azimuthal modulation can be used to target exposure reduction to certain organs. For example, to reduce radiation dose to the eyes during a head scan or to the breasts during a chest scan, the azimuthal modulation can be modified to further reduce the mAs during the AP projection and compensate with increasing mAs for the lateral and/or PA projections.

In practice these three techniques may be available as separate options or activated together as part of an automated scanning mode, depending on the manufacturer's implementation. Some manufacturers have extended this concept further by providing organ-specific boost functions (to fine-tube target noise values in specific anatomic regions) and enabling the operator to automate the selection of tube kV based on the patient attenuation determined from the scout image(s).

Dual-Energy/Spectral Acquisition

Transmission measurements in conventional CT are a physical measure of the linear attenuation properties of tissue, as described earlier. Linear attenuation depends on two underlying properties—density and atomic number—that cannot be measured separately in a single transmission measurement. However, if a sample's transmission is measured using two different beam spectra, the two different attenuation measurements can be used to separate the two components of attenuation.

This property can be useful to probe the chemical composition of a sample. For example, a blood vessel containing iodinated contrast attenuates x-ray much more strongly than a vessel with contrast-free blood, although both have about the same density. The k-edge of iodine (determined from its atomic structure) makes it a strong attenuator. If the two vessels were imaged in a dual-energy mode and information about the physical density were recovered (independent of the atomic structure effects), the two vessels would appear to have about the same attenuation. Similarly the chemical composition of solids such as renal calculi can be probed with multiple x-ray energies to assess the content and composition of calculi having similar physical densities.

The most promising applications for dual-energy and spectral CT capabilities are virtual noncontrast (VNC) exams, iodine quantification, and calcium quantification. Dual-energy/spectral reconstructions can also prevent beam hardening artifacts and related errors in attenuation quantification (HU values).

There are several commercially available CT scanner design implementations that provide options for dual-energy or spectral CT scanning.

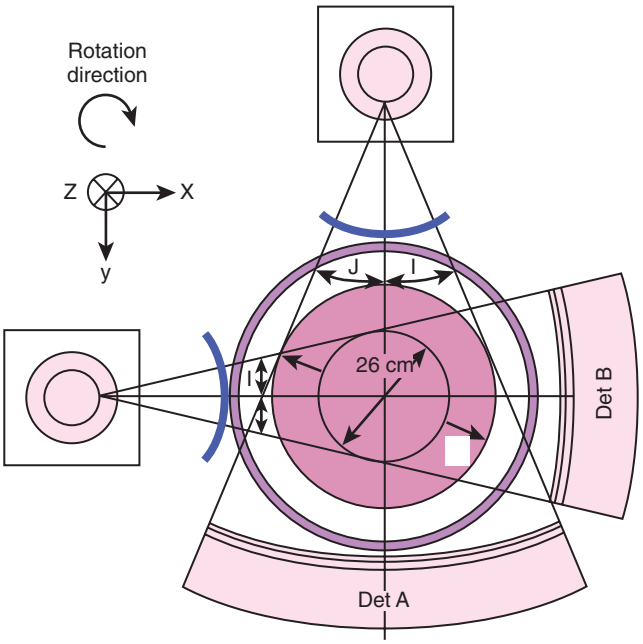

FIG 1-11 Configuration of a dual-source CT scanner. (Courtesy Siemens Healthcare.)

DUAL SOURCE

The dual source scanner employs two complete imaging assemblies, each consisting of an x-ray tube and detector array mounted at right angles to one another and aligned to scan the same plane simultaneously (Fig. 1-11). This approach increases the amount of azimuthal detector coverage so that 360-degree sampling can be achieved with a partial revolution of the scanning frame; for very fast rotations, this greatly increases scanning speed. Each x-ray tube can be operated at a different kV and mAs setting, and the data from the two detector arrays can be stored separately, so it is straightforward to enable the dual-source scanner to operate in a dual-energy mode. A typical approach would be to operate one tube at 80 kV and the other tube at 140 kV.

The dual-source approach has several limitations. First, the second detector covers a smaller arc than the main detector, so the FOV is limited for any dual-source scan (whether high-speed or dual-energy). Second, the data collection for each of the two detectors is offset from the other by a quarter rotation (in space and time), so the two energy measurements are not simultaneous. There can be misregistration between the two energy images if there is patient motion during the scan.

Fast kV Switching

Scanners that use fast kV switching to provide dual-energy scanning have special x-ray generators (discussed earlier) capable of alternating the kV to the x-ray tube approximately every 150 ms so that data for the two spectra are acquired for interleaved azimuthal projections during the tube rotation. A typical acquisition would involve toggling between 80 kV and 140 kV. The data acquisition is synchronized to the kV switching so that the high- and low-energy data are stored separately to produce two different attenuation measurements in the tissue.

Fast kV switching does not provide truly simultaneous acquisition of the two spectral measurements, but there is less spatial and temporal offset than in dual source. A fast kV switching scan would thus be less prone to misregistration between the two energy scans due to motion. Fast kV switching dual-energy scanning requires that the detectors contain scintillators with very fast light decay to prevent crosstalk between the energy measurements. In current commercial systems, the x-ray generator is not able to provide tube current modulation in fast kV switching modes, so manual tube current selection must be used, forgoing some tailoring of radiation exposure to the patient.

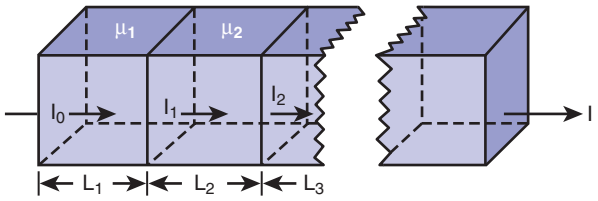

FIG 1-12 Attenuation of photon beam through successive thicknesses of tissue.

Dual Detector

The dual detector approach uses a dual-layer detector exposed to a single x-ray beam. Because the beam has a wide energy spectrum, the top detector layer detects the low-energy photons, while the higher-energy photons pass through the top layer and are detected in the bottom layer. The detector is characterized to determine which portion of the spectrum is detected by each layer. The signals from the two layers are stored separately to provide two distinct energy-related transmission measurements.

Unlike dual source and fast kV switching approaches, there is no need to prospectively select dual-energy operation with the dual layer detector. Every scan is inherently acquired in two detector data sets. At reconstruction these data can be combined into a conventional transmission measurement or used separately to recover density and composition information. In the dual-layer detector, all of the energy measurements are simultaneous for each projection, so there is no misregistration between the spectral signals due to motion. The major drawback to the dual-layer detector approach is that there is a large overlap in the spectra to which the top and bottom layers are sensitive, which degrades the ability to decompose the acquired data into material properties and accurately quantify the atomic number and density of species in the sample.

RECONSTRUCTION

Basic Principles

Reconstruction produces an image from the digital data, representing the attenuation coefficients of the tissue voxels, provided by the data acquisition system. The acquired scan data are composed of a large number of individual ray attenuations.

Figure 1-12 shows a simplified diagram of an x-ray beam passing through successive slabs of tissue. The exit intensity from the first slab is the entrance intensity of the second slab, and so forth. To simplify this example, we assume that each of the slabs has the same thickness ($L_1 = L_2 = \ldots L_n$) and the same linear attenuation coefficient μ, so that the equation for the transmitted beam passing through the n slabs is written as:

$$I = I_0 e^{-\mu L}$$

where:

$\mu L = \mu_1 L_1 + \mu_2 L_2 + \ldots \mu_n L_n$

If we now take the natural logarithm (ln) of both sides of the transmitted beam equation and rearrange it, the result is:

$$\mu = (\mu_1 + \mu_2 + \ldots \mu_n) = \frac{1}{L} \ln \frac{I_0}{I}$$

This equation shows that if the transmission (ratio of incident intensity I_0 to transmitted intensity I) and path length L are known, the sum of the attenuation coefficients along the path of the x-ray beam can be calculated. In a CT scan, the transmission is measured and the distance from the source (x-ray tube) to the detector is known. Each projection then provides a measurement of μ. In a real sample, each incremental thickness of tissue does not have the same attenuation as each other one, and a projection only measures the sum of many tissues along the path. By measuring other projection views along different angles (paths), the individual elements that make up a path can be deduced from the other paths that cross it when other view angles are sampled.

Filtered Backprojection

The simplest and most common method of producing a cross-sectional image from CT data is called *filtered backprojection* (FBP).[19] This method is relatively fast and can be used to reconstruct a large number of images in a few seconds using modest computing resources. In FBP, a mathematical operation is applied to the projection data to extend each 1D projection radiograph into a 2D image. This is the "backprojection" of the 1D data into a 2D map. The 2D images are superimposed over each other, each oriented in the direction of the projection that was used to produce it. This process is illustrated in Figure 1-13. Some blurring always occurs because when each view angle is backprojected, the operation assumes that the measured attenuating material is uniformly distributed across the entire FOV; in reality, the attenuating material is localized somewhere within the FOV.

Filtering is applied to the data to help reduce the blurring due to backprojection. The filtering procedure consists of operating on the ray data with a filter function or convolution kernel. The filter function is a complex one that depends on many parameters, including x-ray tube geometry and detectors. It can take on a number of forms depending on the desired result. For example, one type of filter function might enhance edges and thus sharpen the image, whereas another would blur edges for more gradual density changes. The edge-sharpening filter enhances spatial resolution but simultaneously decreases density resolution. Also, filters that preserve (or enhance) greater detail also result in a noisier reconstructed image. Filters that introduce some blurring also have the effect of smoothing, which reduces noise in the reconstructed image.

FBP of data acquired in helical scanning modes requires special treatment because the patient is moved continuously through the scan plane during data acquisition. If the data over a 360-degree rotation were reconstructed as in conventional (axial) CT, motion artifacts due to the movement of the table or patient would be visible.

To minimize these artifacts and reconstruct a planar image anywhere throughout the volume of collected data, some data must be synthesized or interpolated. The simplest form of interpolation is *linear*. Before reconstruction, projection data are weighted to produce individual sections of data at select locations. Spiral interpolators apply weighting factors to segments of the spiral data to estimate the data that would have been measured if an axial scan had occurred at a particular location.

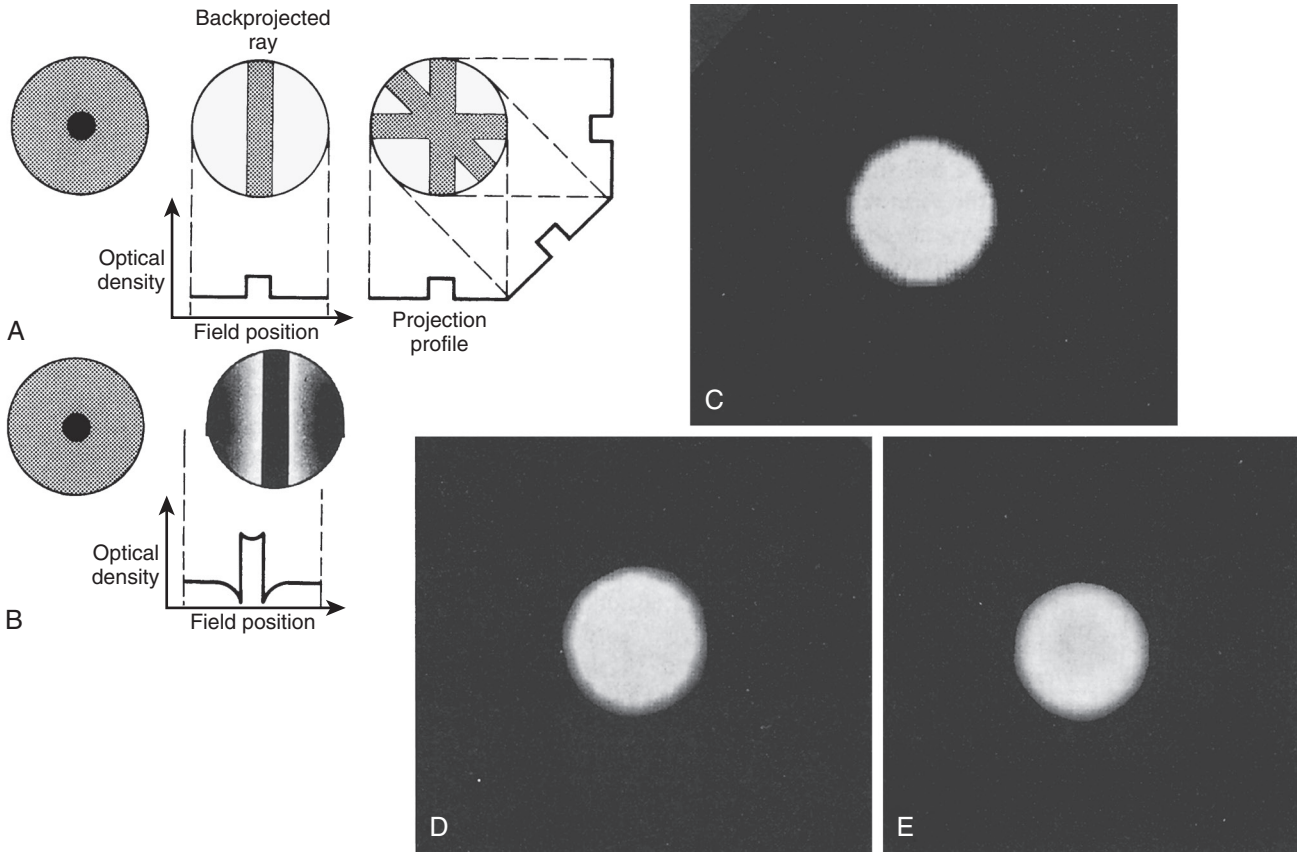

FIG 1-13 Filtered backprojection concept. **A,** Object in center of field of view, backprojection of one view, and backprojection of three views sampled on different view angles. **B,** Backprojection of one view angle with filtering applied. **C-E,** Reconstructed image of the simulated object acquired using 18, 36, and 72 views, respectively.

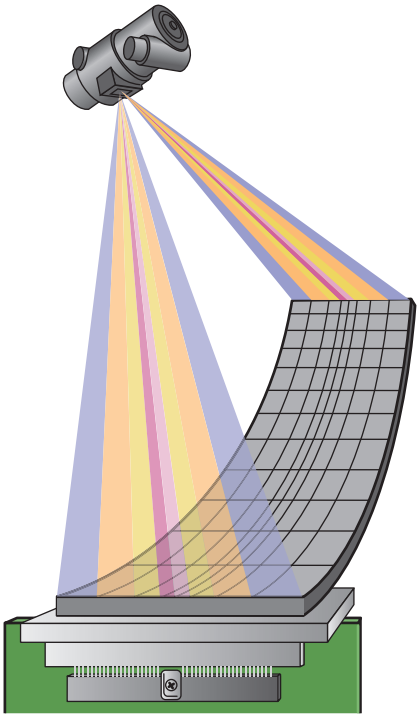

FIG 1-14 Cone-beam geometry in multidetector-row CT. The x-ray beam diverges along the z-axis, and the source-detector length is significantly different for central and outer detectors.

In multidetector-row CT, the fan-beam reconstruction techniques used by conventional and spiral CT must be modified to account for the divergence of the fan beam along the longitudinal axis (z-axis), which creates a *cone-beam* shape (Fig. 1-14). The cone-beam effect results from the source-detector geometry; there is a significant difference between the distance from the x-ray focal spot to the center detector row and the distance from the focal spot to the outer detector rows. This effect is more severe for wider detector arrays. If the number of rows of detectors is limited to a small number (e.g., four rows) of narrow detector-row widths (e.g., 1.5 mm), the cone-beam divergence is very small relative to the resolution of the detector element.

One of the weaknesses of FBP reconstruction in general is that there is an inverse relationship between image noise and radiation dose to the patient. As radiologists seek to lower the radiation dose delivered to patients without degrading image contrast and detail, new methods have been developed to work around these limitations. Iterative reconstruction techniques have been in common use in nuclear medicine (single-photon emission computed tomography [SPECT] and positron emission tomography [PET]) for some time, but the number and size of the image files are much smaller for those modalities. Iterative reconstruction was not viable for CT until recent advances in computing enabled iterative reconstruction of CT data sets in times short enough to be feasible for clinical use.

Iterative Reconstruction

Iterative reconstruction (IR) is a name for a broad class of methods that have general similarities.[2,11,12,44,58,60,61] There are many distinct implementations that have been developed; a detailed description of all of these methods would occupy an entire textbook by itself. Here we focus on the general principle of how IR works and the clinical utility of IR for CT imaging.

The most basic approach to IR is very different from FBP. The projection data are stored but are not backprojected. Instead the computer generates a "guess" image. This image is digitally forward-projected—simulating the process of CT scanning—to produce a set of projection data from the guess image. Next the projection data are compared to the real projection data acquired during the scan (usually by subtraction) and a difference data set is generated. The difference data are used to update the guess image. Then the cycle starts again; the new guess image is forward-projected, and so forth. This process continues until a preset number of iterations are completed or until the reconstruction converges. This is determined by the difference data containing small enough values for the latest guess image to be considered "equal" or "close" to the physical sample represented by the acquired data.

It is interesting to note that in this simplified theoretical implementation of IR, the sampled data are not directly reconstructed; they are used as a reference for comparison but are not backprojected. This is not true of all commercial implementations of IR. These methods introduce the sampled data into the process in some way, such as blending the IR results with FBP image data reconstructed from the acquired data. The noise in CT is contained in the acquired projection data; it is either a product of random statistical photon noise in the x-ray beam nor electronic noise introduced by the scanner's electronics. Thus the noise can be reduced in methods that use the acquired data to guide formation of the image by means other than reconstructing it directly.

Qualitative comparisons of FBP and IR images generally note that the image characteristics differ in ways other than the noise amplitude. IR processing introduces different spatial characteristics into the image than FBP. Quantitatively these are shown as differences in the *noise power spectrum* (NPS) of each reconstructed image type.[45] Qualitatively these feature differences are sometimes described as differing *image textures*.[16] Matching or comparing IR and FBP images based on characteristics such as noise, signal-to-noise ratio (SNR), contrast-to-noise ratio (CNR), and spatial resolution (detail/blurring) would not fully describe the observed differences in image appearance that arise from these reconstruction and NPS differences.

DATA DISPLAY AND MANAGEMENT

Image display includes all the system components necessary to convert the digital data provided by the reconstruction system to electrical signals used by the display monitor, enabling a graphic display of individual CT numbers representing attenuation values of individual sections of anatomy.[8] In addition the display system includes the ability to display patient information, scan protocol, and reconstruction parameters, and it provides the user with many graphic aids to assist in the interpretation of clinical images.

In Figure 1-15, a wide window display setting at left shows all the tissues but minimal contrast within and between them. The image at the right uses a narrow window setting that emphasizes contrast within the liver while saturating other tissues to white or black pixels.

Multiplanar Reformatting

Because a conventional CT study consists of several contiguous axial images perpendicular to the long axis of the body, coronal or sagittal images are not possible to acquire directly unless the gantry is tilted or the body is positioned to show the image in the desired plane. This limitation of CT can be overcome by image manipulation commonly referred to as *multiplanar reformatting* (MPR). In this process, image data are taken from several axial slices and reformatted to form images in another plane. In this viewing mode, the user defines the number of imaging planes and their position, orientation, thickness, and spacing, and the reformatted image is displayed in sagittal, coronal, or

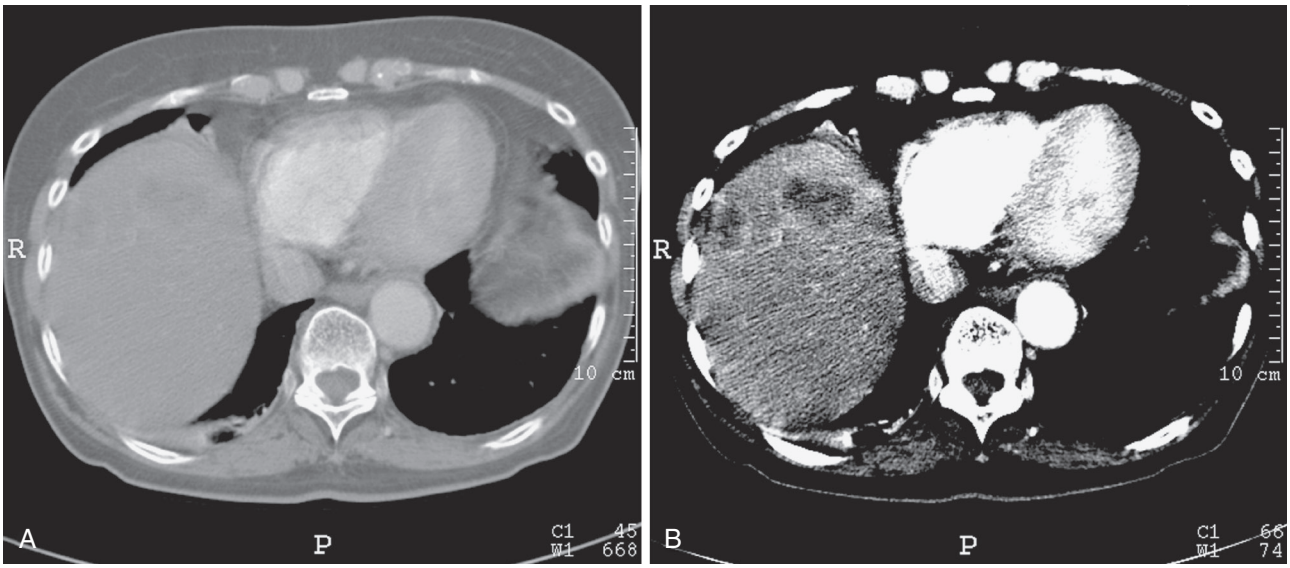

FIG 1-15 Liver scan. **A,** Wide window setting; some lesions are not readily visible. **B,** A more appropriate window setting improves the visibility of lesions. (Courtesy Dr. John R. Haaga.)

oblique planes. In the x-y plane direction, the pixel of the reformatted image has the same length as the axial image; in the z-axis direction, however, the pixel length is the same as the slice thickness. Because in most scans the pixel length is considerably smaller than the slice thickness, the reformatted scan can have an unusual appearance (Fig. 1-16). The resolution is good in one direction in the image plane but very poor in the other. This problem can be addressed by scanning with a smaller slice thickness; also, as described earlier, the image is best enhanced with the use of spiral/multislice CT scanning, in which longitudinal resolution permits a slice thickness resembling minimal pixel length in the x-y plane. Scanning in this mode is commonly referred to as *isotropic imaging*. Isotropic voxels permit increased visualization of complex anatomic shapes that do not run linearly along the z-axis (patient axis).

Data from successive slices can also be reformatted to generate other viewing modes; 3D shaded surface (Fig. 1-17), volume rendering, and maximum intensity projection (MIP) are a few examples. Each of these rendering techniques will be described in detail.

Figure 1-18A illustrates a small segment of eight voxels representing a large-volume data set for demonstration purposes. Each of the eight voxels is shown with its values displayed. A viewpoint is defined from where imaginary rays are projected. To simplify the example, we can assume that each ray intersects two voxels, one behind the other.

Three-Dimensional Shaded Surface

For a surface rendition, the user selects a threshold range (see Fig. 1-18B). This allows the user to select only the tissue (e.g., bone) to be rendered. The voxels with Hounsfield values within the threshold range are set to the "on" state, whereas the rest of the voxels are set to the "off" state. Depending on the number of bits used for display, "on" and "off" voxels are assigned appropriate values. For an 8-bit display, "on" would be 256 and "off" would be 0.

The second step is to project rays through the entire volume. As the rays pass through the data, they stop when they identify the first "on" voxel. For that particular ray, this first "on" voxel is part of the surface; the other voxels are ignored. This is done for all the rays, and all of the "on" voxels are used to create the surface. For our example, the "on" voxels that are part of the surface would be yellow in Figure 1-18C. As the name suggests, only a surface is displayed in this method; there are no details below the surface. Shading the voxels enhances the effect so that the volume image appears to be illuminated by light sources. Multiple light sources can be used, but a single light source is used in most medical applications.

Three-Dimensional Depth-Based Shading

One type of shading technique is called depth-based shading. With this method, those voxels that are closer to the viewer are illuminated at a greater intensity than those that are farther back. As described earlier, it is also possible for the operator to select a range of CT numbers to display. If an operator were interested in a 3D view of the skull, he or she would select the range of CT numbers of the skull. The computer would then assemble those selected voxels into a 3D image. The result is a reconstructed 3D image of the skull with the soft tissue removed.

As with sagittal and coronal images, the quality of the image is improved by interpolating the data between slices to form a smooth continuous image. When various 3D views are selected sequentially in time, the image can appear to rotate. These images pose the same challenges as do sagittal and coronal images. The vertical resolution is the same as the slice thickness and not nearly as good as it is in other directions. Thus spiral/multislice CT dramatically improves 3D viewing because of its ability to cover the same anatomy as a conventional CT scan at much thinner slice thicknesses and with overlapped image reconstructions.

Volume Rendering

Another possible viewing mode is compositing/volume rendering (VR). VR is an advanced rendering technique that displays an entire volume set with control of the opacity or translucency of selected tissue types. In this case, each voxel has an associated intensity in addition to an associated opacity value. Figure 1-19 shows the same 8-voxel block as Figure 1-18A, with each voxel having an opacity value associated with it. The user can define the opacity values for various HUs.

Once the opacity values are assigned, the second step is to pass rays through the volume, accumulating values along the way. The value for each voxel is determined using the intensity value of the voxel and the opacity selected by the user. Figure 1-20 demonstrates the results of this technique for the simplified example.

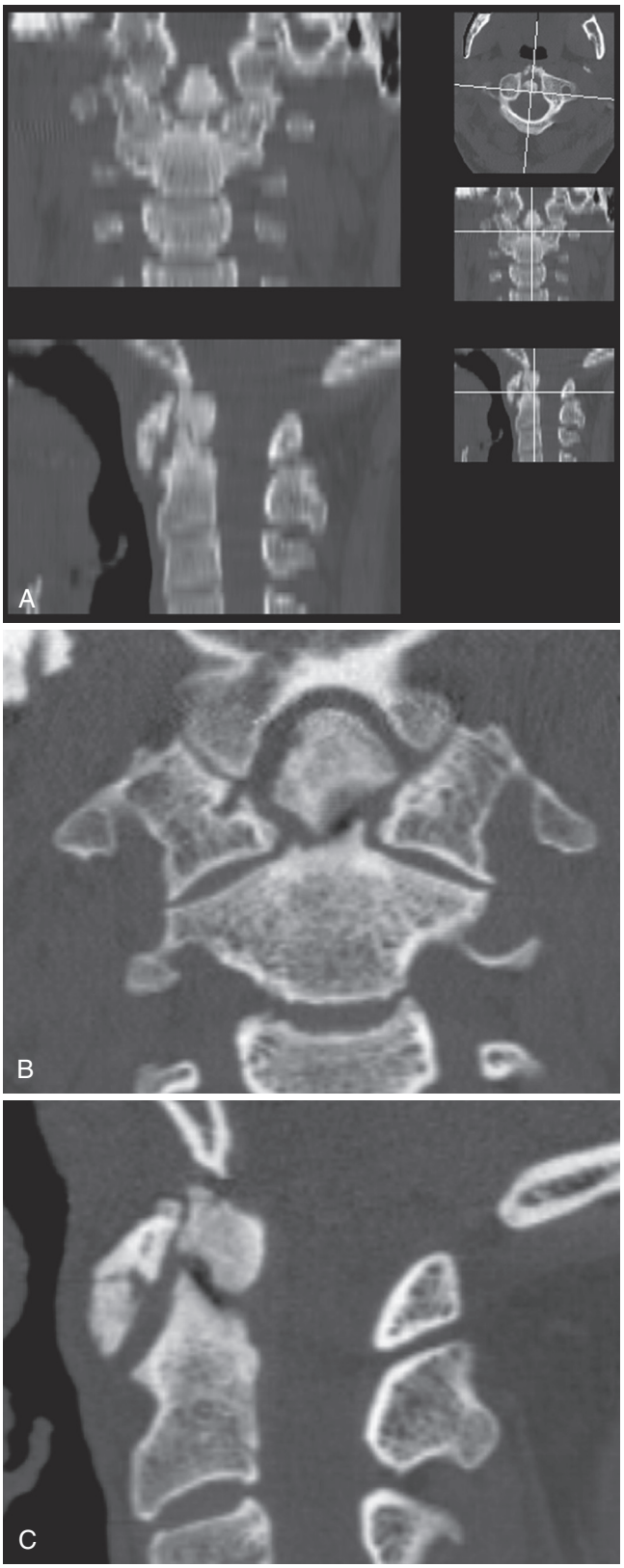

FIG 1-16 Multiplanar reformatting of CT images of the cervical spine. **A,** Multiplanar reformatted images acquired with a slice thickness of 2.5 mm, showing stair-stepping artifacts. **B** and **C,** Multiplanar reformatted images acquired with slice thickness of 0.5 mm (isotropic resolution). (Images courtesy Dr. Jay Cinnamon.)

FIG 1-17 Shaded-surface view of coronary arteries presented as a "soap bubble" view. Such views permit better visualization of the overall paths, but as with any reconstructions, meticulously executed algorithms are essential to prevent artifacts. (Courtesy Philips Medical Systems.)

The obvious advantage of VR over 3D shaded-surface rendering is that it provides volume information. By using transparency, the operator can visualize information beyond the surface. For example, VR is the preferred viewing mode for stent evaluation, because stents can be made transparent to view the lumen of vessels. Other clinical examples include the ability to make plaque transparent for more accurate diagnosis of vessel stenosis.

Maximum Intensity Projection

Using maximum intensity projection (MIP) for visualization permits easy viewing of vascular structures or air-filled cavities.[13] Compared with 3D or volume rendering techniques, MIP is a relatively simple method. Unlike 3D shaded-surface and VR displays, no preprocessing is required. The rays are cast throughout the volume, and depending on whether it is MIP or minimum intensity projection, maximum or minimum values along the rays are used in the final image display. On the basis of the 8-voxel example described earlier, Figure 1-21 shows the final pixel values for MIP and minimum intensity projection.

MIP is a preferred method for many CT angiography applications for visualization of contrast-filled vasculature. MIP enables easy viewing of an entire vessel in one image. This is because voxels representing the contrast-filled vessels are most likely to be the ones with the highest values along the ray (assuming no bone along the ray). Similarly, minimum intensity projection can be used to visualize air-filled cavities.

IMAGE QUALITY

Quantitative Measurements

Several quantitative measurements are used to define a CT system's image quality: spatial resolution, contrast resolution, image noise, and temporal resolution. Image quality is also related to the radiation dose used to produce the image.

Spatial Resolution. *Spatial resolution* is measured by the ability of a CT system to distinguish two small high-contrast objects located very close to each other under noise-free conditions. Optimal spatial

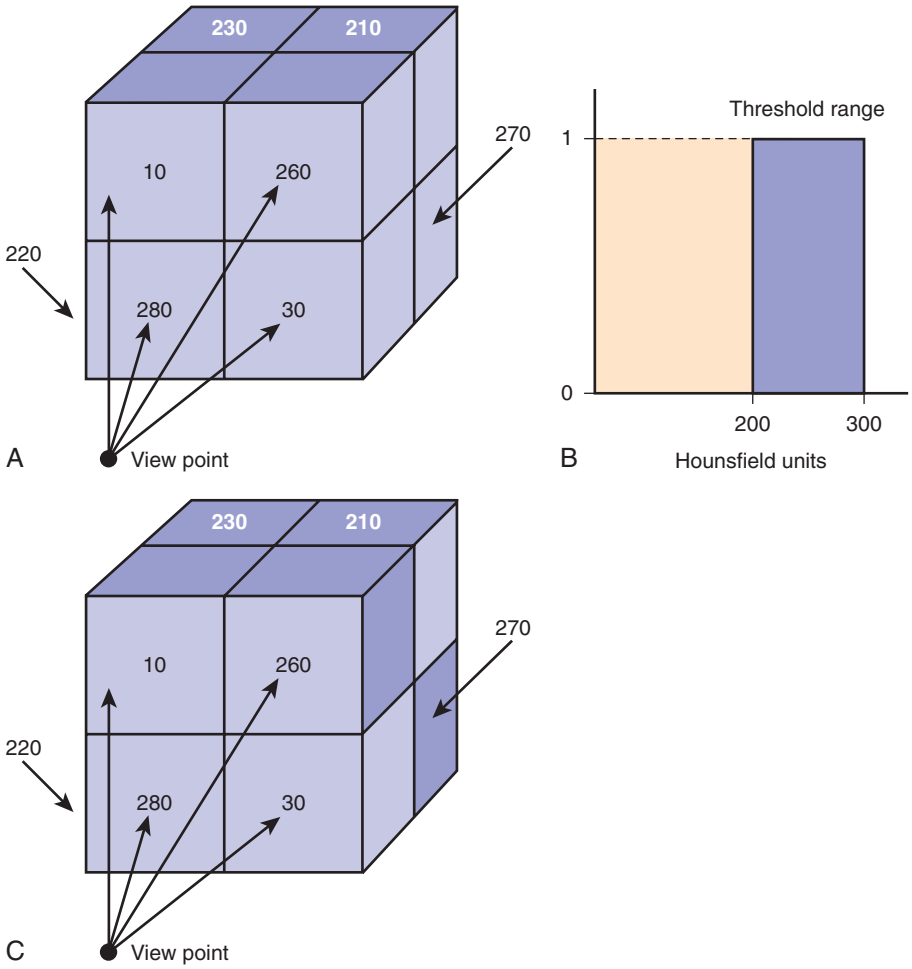

FIG 1-18 **A,** Sample of 8-voxel data set with displayed CT number values. **B,** User-defined threshold of CT number values for tissue definition. **C,** Shaded voxels represent defined tissue surface (shaded-surface display). (Courtesy Shalabh Chandra, Philips Medical Systems.)

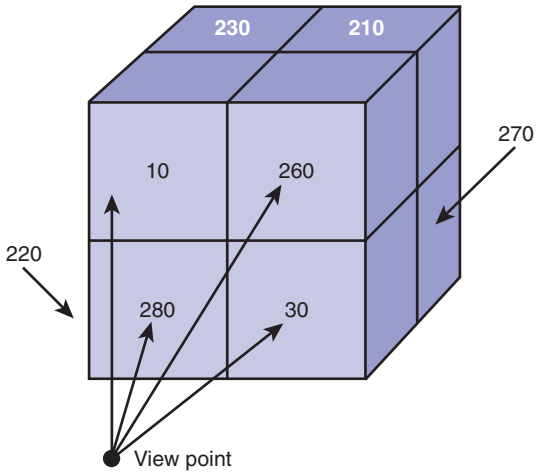

Opacity values for the voxels are given by:
HU < 50. $\alpha = 0.0$: $50 \leq$ HU < 200. $\alpha = 0.2$: $200 \leq$ HU. $\alpha = 0.5$

FIG 1-19 Sample of 8-voxel data set with representative opacity values assigned to various CT number ranges. (Courtesy Shalabh Chandra, Philips Medical Systems.)

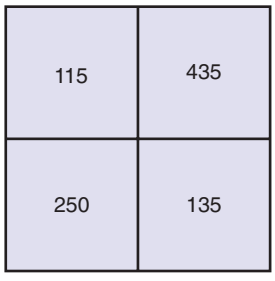

Volume rendered, 4-D angio, composited

FIG 1-20 Image results for volume-rendered image of Figure 1-19.

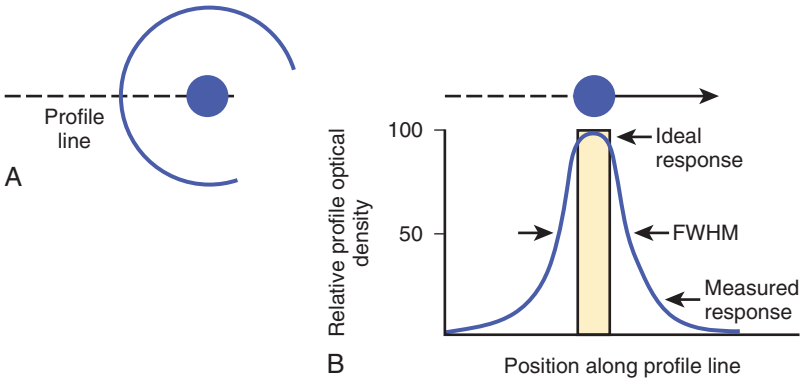

FIG 1-21 Full width at half-maximum (FWHM) demonstrated for a point source. **A,** Solid body in uniform medium. **B,** Profile across the image demonstrates the fading periphery of the image of the solid body. The rectangular profile represents an ideal response with perfectly sharp edges.

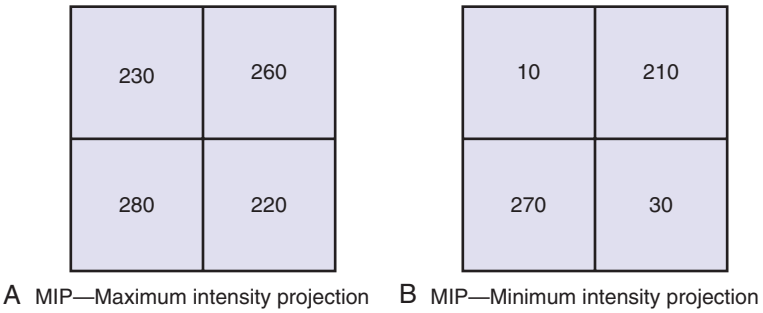

FIG 1-22 **A,** Maximum intensity projection of a sample voxel in which only maximum values are displayed. **B,** Minimum intensity projection in which only minimum values are displayed.

resolution is required for evaluating high-contrast areas of anatomy (e.g., inner ear, orbits, sinuses, bone) in general because of their complicated shapes.

Spatial resolution can be specified by spatial frequencies, which indicate how efficiently the CT scanner represents different frequencies. Modulation transfer function (MTF) describes this property. A 2D Fourier transform of the point spread function taken with a very thin wire provides MTF values. These concepts are described next.

Consider the image of a point source that can be obtained by placing a thin wire on end in water or plastic and then scanning across the wire. Ideally the resulting image should be a uniform background with a bright dot denoting the position of the wire. In fact the image does demonstrate the bright dot but with a fading periphery rather than an absolutely sharp edge. A profile across the image (i.e., a plot of the picture density along a line passing through the point source center) produces a bell-shaped distribution called the *point response distribution.* The height of this curve represents the maximum value of the density, and the width represents the uncertainty in the measurement of the exact boundaries of the wire.

Full width at half-maximum (FWHM) is the width of the curve at the point where the attenuation values are 50% of the peak value (Fig. 1-22). The smaller the FWHM, the better the resolution. One can appreciate this fact by noting that a large FWHM reflects a larger fading periphery, which means a poorer reproduction of the actual object.

Another method of examining spatial resolution is to consider line images. This is similar to examining point images, but the scan would be done parallel to a wire in a medium rather than across the axis. If a series of lines of different spacing or different sizes were used, the ability to distinguish separate lines in an image would measure the spatial resolution. With very fine lines a measure of the resolution can be stated in terms of the number of lines that are still discernible, packed together in a given distance. Thus one would speak of the number of lines per centimeter that could be visualized in the image. Describing the spatial resolution in terms of lines per centimeter is said to describe the resolution in the frequency domain. The frequency in this case is the parameter *lines per centimeter.* A profile across the line image yields the line response curve, which is similar to the point response curve. Again, one can speak of FWHM and the analysis is similar to that done with the point source. Obviously the two response curves are related.

Performing a mathematical operation, the Fourier transform, on these response curves yields the MTF. The physical interpretation of the MTF is that it defines the relative fidelity of the image compared with the actual object.

Another description of the MTF is shown in Figure 1-23. The rectangular profile represents the density profile of an object composed of dense lines. The density profile of the reconstructed image is shown as rectangles with rounded corners. As the lines become closer together, the region between lines fills in because of the overlap of the response functions.

The ratio of the height of the rectangles to the height of the valley between lines becomes smaller as the lines become closer in the reconstructed image, but obviously the ratio is fixed in the object. This change or decrease in ratio is seen as a decrease in contrast and is a manifestation of the decreasing ability of the system to resolve small objects (or small separation of objects). The MTF is basically the value of this ratio in the image divided by the value of the ratio in the object. As the frequency increases (i.e., more lines per centimeter) the ability of the system to reproduce the lines and valleys accurately is decreased and the fidelity also therefore decreases.